

Novel AAV44.9-Based Vectors Display Exceptional Characteristics for Retinal Gene Therapy

Sanford L. Boye,¹ Shreyasi Choudhury,² Sean Crosson,² Giovanni Di Pasquale,⁴ Sandra Afione,⁴ Russell Mellen,² Victoria Makal,² Kaitlyn R. Calabro,² Diego Fajardo,² James Peterson,² Hangning Zhang,² Matthew T. Leahy,³ Colin K. Jennings,³ John A. Chiorini,⁴ Ryan F. Boyd,³ and Shannon E. Boye²

¹Department of Pediatrics and the Powell Gene Therapy Center, University of Florida, Gainesville, FL, USA; ²Department of Ophthalmology, University of Florida, Gainesville, FL, USA; ³Ophthalmology Services, Charles River Laboratories, Mattawan, MI, USA; ⁴Adeno-Associated Virus Biology Section, National Institute of Dental and Craniofacial Research, National Institutes of Health, Bethesda, MD, USA

The majority of inherited retinal diseases (IRDs) are caused by mutations in genes expressed in photoreceptors (PRs). The ideal vector to address these conditions is one that transduces PRs in large areas of retina with the smallest volume/lowest titer possible, and efficiently transduces foveal cones, the cells responsible for acute, daylight vision that are often the only remaining area of functional retina in IRDs. The purpose of our study was to evaluate the retinal tropism and potency of a novel capsid, AAV44.9, and rationally designed derivatives thereof. We found that AAV44.9 and AAV44.9(E531D) transduced retinas of subretinally injected (SRI) mice with higher efficiency than did benchmark AAV5- and AAV8-based vectors. In macaques, highly efficient cone and rod transduction was observed following submacular and peripheral SRI. AAV44.9- and AAV44.9(E531D)-mediated GFP fluorescence extended laterally well beyond SRI bleb margins. Notably, extrafoveal injection (i.e., fovea not detached during surgery) led to transduction of up to 98% of foveal cones. AAV44.9(E531D) efficiently transduced parafoveal and perifoveal cones, whereas AAV44.9 did not. AAV44.9(E531D) was also capable of restoring retinal function to a mouse model of IRD. These novel capsids will be useful for addressing IRDs that would benefit from an expansive treatment area.

INTRODUCTION

Recent US Food and Drug Administration (FDA) approval of an adeno-associated virus (AAV)-based gene therapy for RPE65-Leber congenital amaurosis (LCA2) solidified gene therapy's place in current medical practice. The early success of this program fueled additional studies that established proof of concept for gene replacement therapy in models of other retinal diseases, including, but not limited to, choroideremia, achromatopsia, and X-linked retinoschisis. Notably, however, these exciting preclinical results have not consistently produced the robust clinical outcomes seen in LCA2.¹⁻³ One of the obstacles to overcome is achieving sufficient transgene expression in the target cells of the retina while avoiding dose-limiting toxicity and/or iatrogenic pathologies. Because most inherited retinal diseases (IRDs) are caused by mutations in photoreceptor (PR)-specific genes, development of gene replacement strategies that can more

safely and efficiently target these cells is still a significant, unmet need. The ability to effectively target foveal cones is especially important, as they are responsible for acute, daylight vision.

Intravitreal injection (IVI) is a promising approach for treating fragile, degenerate retinas that are prone to additional damage upon surgical detachment, but it requires an AAV capsid capable of "penetrating" through the retina from the vitreous. IVI is attractive because it can be performed in the clinic rather than a surgical suite, thereby increasing accessibility of gene therapies to larger patient populations. However, the limited clinical data,^{2,3} and non-human primate (NHP) studies⁴ utilizing currently available capsids, indicate that the barriers to IVI AAV (i.e., dilution/neutralization in vitreous, inner limiting membrane) restrict gene expression to levels that are "sub-therapeutic" in a proportion of patients. Even with enhanced AAV vectors, IVI-mediated transduction is currently limited to retinal ganglion cells (RGCs) in the macular "ring," RGCs and Müller glia surrounding large blood vessels, some foveal cones, and non-neuronal cells of the ciliary body.^{5,6} Clinical trials using IVI AAV are nevertheless underway or planned for the treatment of both dry and wet age-related macular degeneration. Patients may be excluded from these trials or be refractory to treatment due to pre-existing neutralizing antibodies (NAbs) to AAV.⁷ For these reasons, subretinal injection (SRI) may still be the optimal injection route for many IRD indications. While SRI of AAV vector under the LCA2 patient fovea led to central retinal thinning and loss of visual acuity in some patients,⁸ other retinal diseases characterized by severe functional deficits in spite of retinal preservation (e.g., achromatopsia, *GUCY2D*-LCA1) present a better risk-to-benefit ratio for a sub-foveal injection. However, in patients with progressive retinal degeneration who retain central cones/vision (e.g., retinitis pigmentosa), sub-foveal injection presents significant risk. In such cases, extrafoveal SRI of a vector capable of spreading laterally through intact, attached retina

Received 20 January 2020; accepted 2 April 2020;
<https://doi.org/10.1016/j.ymthe.2020.04.002>

Correspondence: Shannon E. Boye, Department of Ophthalmology, University of Florida, P.O. Box 100284, Gainesville, FL 32610, USA.

E-mail: shaire@ufl.edu

to reach the fovea would be ideal. In addition, vectors that spread laterally from the injection bleb would enable treatment of larger areas of retina relative to that achieved with current vectors, which mediate transgene expression primarily within the SRI bleb margins.^{9,10}

Recently, a novel capsid, AAV44.9, was isolated from a laboratory stock of simian adenovirus SV15 taken from normal rhesus monkey kidney cell culture. AAV44.9 efficiently transduces a number of cell types, including salivary gland cells, liver cells, and different types of neurons (e.g., cells of the cortex, olfactory bulb, brain stem, and Purkinje cells of the cerebellum) (J. Chiorini, personal communication). AAV44.9, together with closely related AAVrh.8 and AAVrh.8R, falls between AAV clades E and F.¹¹ Previous reports indicate that AAVrh.8R efficiently transduces photoreceptors of SRI mice,¹² and that it has tropism for both rods and cones in SRI macaques.¹³ Other reports indicated that AAVrh.8 was capable of transducing mouse retina following IVI.^{14,15} In the current study, we evaluate retinal transduction and tropism of AAV44.9, and rationally designed derivatives thereof, following IVI and SRI in mice and macaques. AAV44.9 and the AAV44.9(E531D) variant efficiently transduced murine retina following SRI, outperforming benchmark AAV5- and AAV8-based vectors. Notably, when delivered by extrafoveal SRI (i.e., the fovea remains attached during, and after, vector delivery), AAV44.9 and AAV44.9(E531D) transduced up to 98% of foveal cones in macaques. When delivering a reporter construct containing the photoreceptor-specific, rhodopsin kinase promoter (hGRK1), AAV44.9(E531D) mediated efficient expression of the transgene in macaque parafoveal and perifoveal cones, cells that have been refractory to transduction by other AAV vectors.¹³ Additionally when tested in a mouse model of LCA, AAV44.9(E531D) was capable of restoring both cone and rod function following SRI. Our results strongly suggest that these capsids will be useful for treating diseases where the central retina is the therapeutic target, but direct detachment of the fovea is contraindicated. These laterally spreading, potent capsids will also be useful for addressing IRDs where the goal is to treat an expansive area of retina.

RESULTS

AAV44.9 Differs from AAVrh.8 and AAVrh.8R by 3 and 4 aa Substitutions, Respectively

AAV44.9 VP1 differs from AAVrh.8 VP1 (AAO88183) by 4 aa substitutions (AAV44.9 residue first, AAVrh.8 s), that is, T179S, S473N, S483C and E531D (Figure S1). AAVrh.8R differs from AAVrh.8 by one of these variant substitutions, having glutamic acid at position 531 (E531). The VP1 capsid sequence places the group in an intermediate position between clade E and F as grouped by Gao et al.¹⁶ (Figure S1).

AAV44.9-Based Vectors Package Efficiently

Yields of vectors made for this study, as measured in total vector genomes, show that AAV44.9-based vectors compare favorably to benchmark capsids AAV5 and AAV8(Y733F) in terms of manufacturing efficiency. Vectors were manufactured by triple

transfection in adherent HEK293T cells at two different scales, the 1,272-cm² cell growth area (double-stack cell factory) and the 6,360-cm² cell growth area (10-stack cell factory). All vectors were purified by density gradient centrifugation in iodixanol. When comparing identical rAAV genomes packaged, AAV44.9 and AAV44.9(E531D) yields were greater than those of AAV8(Y733F) and AAV6 and were approximately equal to or greater than AAV5, depending on the scale of manufacturing (Table S1). AAV5, AAV44.9, and AAV44.9(E531D) vectors made at the larger scale underwent additional purification by anion-exchange chromatography with a Q Sepharose column using standard conditions outlined by Zolotukhin et al.¹⁷ AAV44.9 and AAV44.9(E531D) vectors were efficiently recovered (data not shown), indicating compatibility to purification by this simple method.

AAV44.9-Based Vectors Outperform AAV5- and AAV8-Based Vectors in SRI Mice

Self-complementary AAV vectors containing the ubiquitous smCBA promoter driving mCherry were evaluated for their tropism and potency in SRI mice. *Nrl*-green fluorescent protein (GFP) mice that express GFP exclusively in rod photoreceptors received an SRI of either AAV44.9, AAV44.9(Y733F), AAV44.9(E531D), AAV8(Y733F), AAVrh.8, AAV5, or AAV2 at concentrations of 2e12 vector genomes (vg)/mL (high dose). AAV44.9, AAV44.9(E531D), and AAVrh.8 were also tested at 2e11 vg/mL (low dose). Fundoscopy performed at 4 weeks post-injection (p.i.) revealed that all vectors efficiently transduced mouse retina following SRI, except for AAV2. By fundoscopy, mCherry expression was apparent throughout the area of observable retina of mice injected with AAV44.9 or AAV44.9(E531D) (Figure 1). Qualitatively, these capsids appeared to exhibit “lateral spread” beyond the margins of the subretinal bleb, a feature that we explored in more detail in later macaque experiments. High-dose AAV44.9 and AAV44.9(E531D) transduced 66% and 87% of rods, respectively (Figure 1). Both significantly ($p < 0.0001$) outperformed AAV5 (41%) and AAV8(Y733F) (58%), and they were comparable to AAVrh.8 (85%) at the high dose. Low-dose AAV44.9(E531D) (35%) significantly ($p < 0.0001$) outperformed AAVrh.8 (21%) in rods (Figure 1; Figure S2). AAV44.9(E531D) was also significantly more potent than AAV44.9 at this dose. Fundus images of mice injected with AAVrh.8- and AAV44.9-based vectors reveal “dark patches” surrounded by robust mCherry expression. Analysis of retinal sections revealed that these patches corresponded to areas of retinal degeneration, a known side effect of overexpressing fluorescent reporter proteins in retina.¹⁸ Immunohistochemistry revealed that SRI of AAV44.9-based vectors led to extensive transduction that was primarily restricted to photoreceptors and retinal pigment epithelium (RPE) (Figure 1). Because quantification of photoreceptor transduction in *Nrl*-GFP mice is restricted to rods, an additional experiment was performed to confirm that AAV44.9 and AAV44.9(E531D) also transduced cones. Indeed, SRI of both vectors containing the cone-specific IRBP/GNAT2 promoter¹⁹ driving GFP in C57BL/6J mice promoted efficient expression of transgene in cones (Figure 1; Figure S3). Mutation of surface-exposed tyrosine residues to phenylalanine (Y-F) on the AAV capsid leads to enhanced

transduction of retina.²⁰ We investigated the effect of a Y733F substitution on AAV44.9, as the homologous substitution on AAV2, AAV8, and AAV9 has been found to substantially increase transduction efficiency.^{20–22} To our surprise, we saw no improvement in retinal transduction for AAV44.9(Y733F) following SRI. Taken together, our results indicate that AAV44.9 and AAV44.9(E531D) are highly potent capsids capable of transducing rods, cones, and RPE in SRI mice.

AAV44.9-Based Capsids Transduce ARPE19 Cells with Low Efficiency

Self-complementary AAV vectors containing the ubiquitous smCBA promoter driving mCherry were tested for their ability to transduce the ARPE19 ocular cell line (human retinal pigment epithelial cells) previously found to be more amenable to transduction by neural-trophic capsids such as AAV5 and AAV8.²³ AAV44.9, AAV44.9(E531D), and AAVrh.8 transduced ARPE-19 cells, albeit with lower efficiency than for AAV5 (Figure S4). Our results are consistent with previous reports that neuronal-trophic capsids generally perform poorly *in vitro*.²⁴

AAV44.9 and AAVrh.8 Vectors Inefficiently Transduce Retina following IVI in Mice

It was previously reported that AAVrh.8 transduced mouse inner retina following IVI.¹⁴ Our prior studies and those of others suggest that the ability of AAV to efficiently transduce retina following IVI is dependent on capsid binding to heparan sulfate proteoglycan (HSPG), a constitutive component of the inner limiting membrane.^{25–27} AAVrh.8 was previously shown not to bind heparin at physiologic concentrations of NaCl.¹⁵ We sought to clarify whether AAV44.9 and/or AAVrh.8 vectors efficiently transduced mouse retina following IVI, and to characterize and confirm their respective binding to heparin. *Nrl*-GFP mice received IVI of AAV44.9, AAV44.9(Y733F), AAV44.9(E531D), AAV8(Y733F), AAVrh.8, AAV5, or AAV2 at a dose of 2e9 vg delivered. Fundoscopy and flow cytometry of dissociated retinas revealed that none of these capsids efficiently transduced mouse retina in comparison to AAV2, our benchmark positive control (Figure S5). Heparin binding profiles of AAV44.9, AAV6 (positive control), AAV5 (negative control),²⁵ and AAVrh.8 (negative control)¹⁵ were determined using heparin affinity column chromatography. To further resolve interactions with heparin at or slightly below physiological salt conditions (~330 mOsm), we lowered background buffer osmolarity to 220 mOsm.²⁸ AAV44.9 and AAV44.9(E531D) did not bind heparin and had elution profiles similar to the non-binder control, AAV5. AAVrh.8 displayed weak heparin binding, with a small amount bound to the column and primarily eluting at the lowest solute concentration tested (270 mOsm). This was in contrast to the profile of the control binder, AAV6 (Figure S5). When evaluated at the standard buffer osmolarity, AAVrh.8 did not bind heparin (Figure S5).

Grafting of Heparin Binding onto AAV44.9 Reduces Transduction Efficiency following Subretinal Administration

We engineered a variant of AAV44.9 with an E to K substitution at residue 531, AAV44.9(E531K), that is predicted to bind HSPG²⁹

and assessed its transduction of ARPE-19 cells and mouse retina following IVI. As expected, AAV44.9(E531K) bound heparin and displayed modestly improved transduction of ARPE-19 cells relative to AAV44.9 and AAVrh.8 (Figure S6). Grafting of heparin binding did not result in the ability of this capsid to mediate transduction following IVI. AAV44.9(E531K) did transduce retina following SRI; however, the efficiency was substantially attenuated relative to parent AAV44.9 (Figure S6).

AAV44.9 Promotes Highly Efficient Foveal Cone Transduction when Subretinally Administered to Macaques

Initial results in mice prompted further analysis in a more clinically relevant, foveated primate species, *Macaca fascicularis*. The first goal of our macaque study was to evaluate tropism of AAV44.9 in both the central and peripheral retina following submacular and peripheral SRI, respectively. AAV44.9 containing either the ubiquitous CBA or photoreceptor-specific hGRK1 promoter driving GFP were compared in two eyes, each delivered at a concentration of 1e12 vg/mL (Table S2). Representative longitudinal images show that GFP expression was observable in the AAV44.9-CBA- and AAV44.9-hGRK1-treated retinas at 1 week p.i. (Figure S7). The CBA promoter drove higher levels of observable GFP at this time point. In retinas treated with either vector, the area of GFP expression increased beyond the injection bleb margins during the course of the study (Figure S7). Six weeks p.i., retinas were collected, sectioned, and analyzed for transgene expression. Three blinded observers counted the number of GFP-positive cones and rods in retinal cross-sections that were stained with cone-specific antibody (cone arrestin) (Figure 2). Submacular SRI of AAV44.9-CBA or AAV44.9-hGRK1 resulted in GFP expression in 95% and 97% of foveal cones, respectively, and 96% and 81% of central rods were GFP positive, respectively (Figure 2; Table S3). Parafoveal cones also expressed GFP in eyes that received submacular SRI of AAV44.9-CBA and AAV44.9-hGRK1 (Figures S8 and S9). This is of note because the earliest loss of structure and function resulting from normal aging and IRD often occurs in parafoveal cones,^{30–40} but these cells are refractory to transduction by a variety of other AAV capsid variants.^{13,41} Direct, submacular injections of AAV44.9(E531D) and AAV5 were not performed. Previous work demonstrated that submacular injection of AAV5-hGRK1-GFP delivered at the same concentration (1e12 vg/mL) led to approximately equivalent GFP expression in photoreceptors, including parafoveal cones, to that observed here by AAV44.9 vectors.⁹ Relative to the underlying photoreceptors, which were strongly and uniformly GFP positive, relatively weak/sporadic GFP expression was observed in the RPE of AAV44.9-CBA-GFP-injected eye (Figure 2; Figure S8). Retinas stained with an antibody raised against RPE65 confirmed the structural integrity of RPE in these sections, ruling out that the relatively low GFP expression in this cell layer was due to the absence of RPE cells (Figure S10). In contrast, SRI of scAAV44.9-smCBA-GFP in mice led to robust GFP expression in both photoreceptors and RPE. Possible reasons for this observed difference in RPE tropism by AAV44.9 across species are (1) different (albeit similar) promoters were used (full CBA in macaque versus smCBA in mouse), or (2)

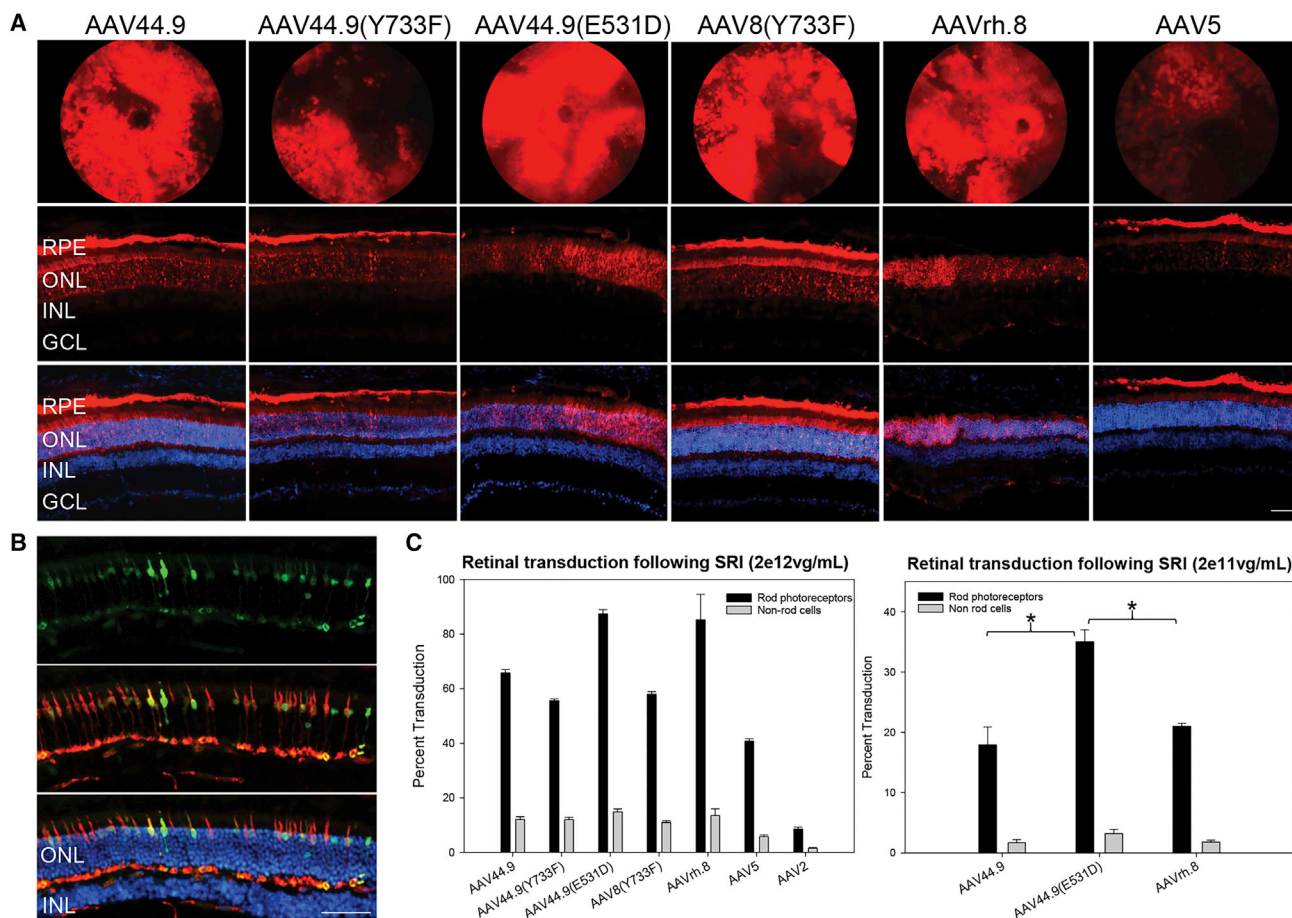


Figure 1. Transduction of AAV Vectors in Subretinally Injected Mice

(A) Transduction profile of AAV vectors following subretinal injection (SRI) in Nrl-GFP mice. AAV-mediated mCherry expression in representative fluorescent fundus images (top row) and retinal cross-sections (middle and bottom rows) taken at 4 weeks post-injection with 2e12 vg/mL is shown. (B) Transduction profile of AAV44.9(E531D)-IRBP/GNAT2-GFP following SRI in C57BL/6J mice. Six weeks post-injection with 1 μ L of 2e12 vg/mL (2e9 vg delivered), retinal cross-sections were stained with an antibody directed against cone arrestin and counterstained with DAPI. Vector-mediated GFP expression and cone arrestin colocalize, indicating that this capsid efficiently transduces cone photoreceptors. (C) Transduction efficiencies as determined by flow cytometry in subretinally injected Nrl-GFP mice. *Kruskal-Wallis tests were performed, followed by a *post hoc* Dunn's test to make pairwise comparisons between groups. For the non-rod values, $H = 44.912$, $df = 6$, and $p < 0.001$. For the rod values, $H = 85.546$, $df = 6$, and $p < 0.001$. Scale bars in (A) and (B), 50 μ m. RPE, retinal pigment epithelium; ONL, outer nuclear layer; INL, inner nuclear layer; GCL, ganglion cell layer.

different vector genomes were used (single stranded in macaques versus self-complementary in mice). Alternative explanations warrant additional investigation.

Peripheral SRI of AAV44.9 and AAV44.9(E531D) Promotes Highly Efficient Transduction of Rods and Cones of Macaques

AAV44.9 and AAV44.9(E531D) vectors also efficiently transduced cones and rods in the periphery (Figure 2). SRI in the periphery (approximately 25 degrees of eccentricity from the fovea) with AAV44.9-CBA, AAV44.9-hGRK1, and AAV44.9(E531D)-hGRK1 resulted in 100%, 97%, and 93% of GFP-positive cones, respectively. 95%, 96%, and 95% of peripheral rods expressed GFP from each respective vector. The same concentration of AAV5-hGRK1 resulted in slightly fewer peripheral cones (89%) and rods (92%) expressing GFP (Figure 2; Table S3). The retinal locations from which peripheral

transduction were quantified are demarcated by arrows in Figure S11. Similar to that observed in submacular injections, the area of AAV44.9- and AAV44.9(E531D)-mediated GFP expression extended outward from peripheral injection bleb margins throughout the course of the study (Figure S7).

Extrafoveal SRI of AAV44.9 and AAV44.9(E531D) Results in Highly Efficient Transduction of Foveal Cones

The second goal of our macaque study was to evaluate whether lateral spread by AAV44.9 and AAV44.9(E531D) would enable transduction of foveal cones without the need for foveal detachment. To do so, three SRIs (average of 30 μ L each) were performed in the superior, temporal, and inferior retina at a distance of approximately 25 degrees of eccentricity from the fovea. Two eyes were injected with AAV44.9-hGRK1, and one eye was injected with either

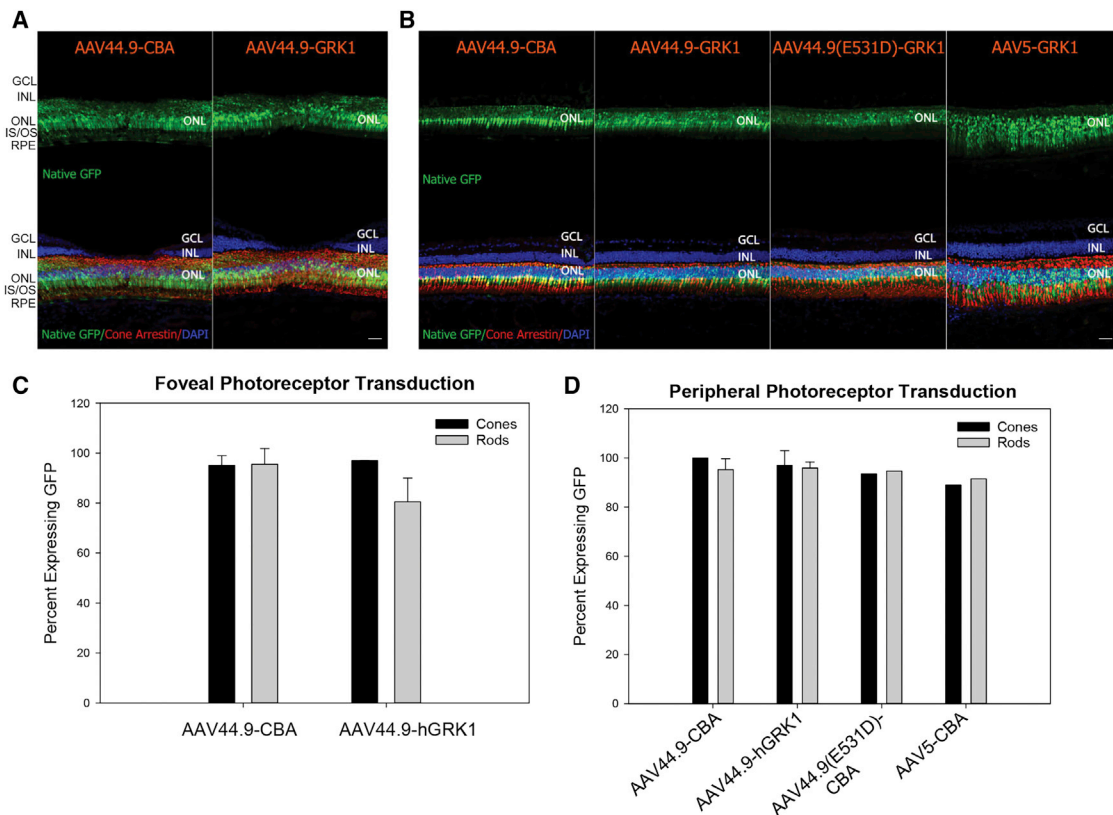


Figure 2. Transduction of AAV Vectors in Subretinally Injected Macaques

Qualitative (A and B) and quantitative (C and D) analyses of GFP expression 6 weeks after submacular or peripheral subretinal injection of AAV44.9, AAV44.9(E531D), or AAV5 vectors (1×10^{12} vg/mL) in macaques are shown. (A and C) Representative confocal images of foveal (A) or peripheral (C) retinal cross-sections stained with an antibody raised against cone arrestin and counterstained with DAPI. Native GFP expression is shown. Images were captured using identical settings. (B and D) Three blinded observers quantified the percent of rods and cones expressing GFP within central (B) and peripheral (D) sections. Scale bars in (A) and (B), 40 μ m. RPE, retinal pigment epithelium; IS/OS, inner segments/outer segments; ONL, outer nuclear layer; INL, inner nuclear layer; GCL, ganglion cell layer.

AAV44.9(E531D)-hGRK1 or AAV5-hGRK1 (Table S2). GFP expression was observed at 1 week p.i. with AAV44.9(E531D), and by 2 weeks p.i. in all eyes (Figure 3). Fluorescence outside the original SRI bleb margins was apparent at 2 weeks p.i. with AAV44.9-based vectors, but not AAV5. Demarcation of retinal vasculature highlighted as landmarks (red lines) reveals that GFP expression extended well beyond the border of the original injection blebs in monkeys treated with AAV44.9 or AAV44.9(E531D), whereas AAV5-mediated GFP expression appears confined to the area of the original injection bleb (Figure 3). The second eye to receive AAV44.9-hGRK1-GFP is shown in Figure S12. GFP intensity mediated by all vectors increased through week 6 (termination), as did the area of transgene expression for AAV44.9 and AAV44.9(E531D). Post-operative fundus photographs (data not shown) and optical coherence tomography (OCT) performed immediately after injection confirmed that foveas remained attached in all treated eyes (Figures 4, 5, and 6).

The percentages of GFP-positive cones and rods were quantified in five discrete retinal regions across a single plane traversing the foveal pit (temporal to nasal). In the AAV5-treated eye, expression was

observed predominantly within the area of the original SRI bleb, with approximately 90% of cones and rods in this region being GFP positive (zone 2, Figure 4). No AAV5-mediated GFP was observed in foveal cones, consistent with the fovea not being detached during the injection (zone 3, Figure 4). AAV44.9- and AAV44.9(E531D)-mediated GFP expression was observed in all retinal regions evaluated, regardless of whether they were located within the original SRI blebs (Figures 5 and 6). Notably, these vectors mediated GFP expression in 96% and 98% of foveal cones, respectively, despite the fact that this region was not detached during surgery. 98% and 100% of central rods were also GFP positive. The lateral spreading behavior of these vectors was also apparent in the zone farthest from the SRI blebs, zone 5 (~1.7 mm nasal to the optic nerve head (ONH), and 5 mm from the foveal pit), with up to 95% of cones and rods transduced in this region. Using the optic nerve head and retinal vasculature as landmarks, we superimposed images of the macular blocks cut for cyrosectioning onto the respective fundus images captured on the day of dosing. This allowed us to approximate distances between the original bleb margins and regions of interest. GFP expression was observable in retinal sections at a distance of

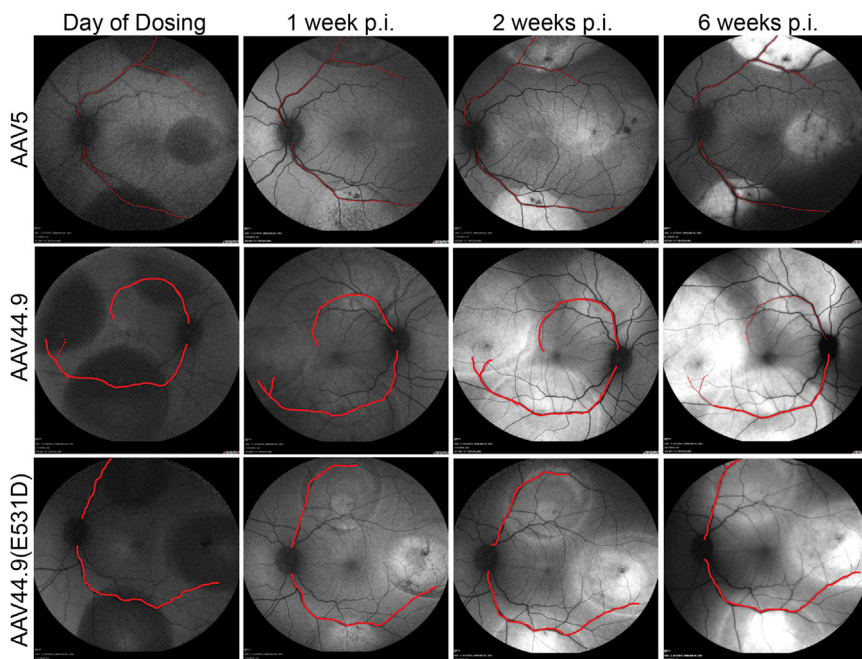


Figure 3. In-Life Assessment of AAV-Mediated GFP Expression in Subretinally Injected Macaques

Confocal scanning laser ophthalmoscopy (SLO) images of macaque eyes that received three extrafoveal subretinal injections (30 μ L each) of AAV5, AAV44.9, or AAV44.9 vectors containing hGRK1-GFP (1×10^{12} vg/mL) are shown. Each injection was initiated approximately 25 degrees away from the foveal pit. Images were taken on the day of dosing and at 1, 2, and 6 weeks post-injection. Red lines are superimposed on retinal vasculature to serve as landmarks.

\sim 6.7 mm from the closest bleb margin in the AAV44.9(E531D)-hGRK1-GFP-injected eye. For AAV44.9-hGRK1-GFP, that distance was \sim 5 mm. AAV5-mediated GFP was found at a maximum of only 1 mm away from the bleb margin.

Comparison of Retinal Structure following Extrafoveal versus Submacular SRI of AAV44.9

A direct comparison indicates that the percentage of GFP-positive cones is virtually identical (97% versus 96%) in the foveas of retinas receiving either submacular or extrafoveal SRI of AAV44.9-hGRK1-GFP (Figure S13; Table S3). OCT analysis revealed a loss of ellipsoid zone and foveal bulge in retinas receiving submacular SRI, consistent with what has been observed before in either surgically induced or rhegmatogenous retinal detachment.^{42,43} These morphological changes either partially or completely resolved by study termination (Figure S14). In contrast, no OCT changes were observed in the fovea of any extrafoveally injected eyes during the course of the study (Figure S15).

AAV44.9(E531D)-hGRK1-GFP Drives Transgene Expression in Parafoveal and Perifoveal Cones following Extrafoveal SRI

As previously mentioned, parafoveal cones are of specific interest in many retinal diseases and have generally been less successfully targeted by AAV vectors. We observed parafoveal cone transduction (both nasal and temporal to the foveal pit) in eyes that received extrafoveal SRI of AAV44.9(E531D)-hGRK1-GFP (Figure 7). Approximately 81% of nasal parafoveal cones and 76% of temporal parafoveal cones expressed GFP in retinal cross-sections. Additional images from this region are presented in Figure S16. This is similar to results previously obtained with AAV5-hGRK1-GFP delivered by submacular SRI.⁹ Notably, however, GFP expression in parafoveal cones was

not observed in retina extrafoveally injected with AAV44.9-hGRK1-GFP. Both AAV44.9 and AAV44.9(E531D) drove efficient GFP expression in rods within this region (Figure 7). We extended our analysis farther out to the periphery and observed a similar pattern; that is, AAV44.9(E531D)-hGRK1 resulted in GFP expression in nasal periphery cones (approximately 89%) and temporal periphery cones (approximately 92%), but AAV44.9-hGRK1 did not (Figure S17). Both vectors led to efficient transgene expression in periphery rods. Parafoveal and periphery areas of retina from which sections were imaged (nasal and temporal) were not contained within the margins of the original SRI injection bleb.

not observed in retina extrafoveally injected with AAV44.9-hGRK1-GFP. Both AAV44.9 and AAV44.9(E531D) drove efficient GFP expression in rods within this region (Figure 7). We extended our analysis farther out to the periphery and observed a similar pattern; that is, AAV44.9(E531D)-hGRK1 resulted in GFP expression in nasal periphery cones (approximately 89%) and temporal periphery cones (approximately 92%), but AAV44.9-hGRK1 did not (Figure S17). Both vectors led to efficient transgene expression in periphery rods. Parafoveal and periphery areas of retina from which sections were imaged (nasal and temporal) were not contained within the margins of the original SRI injection bleb.

AAV44.9(E531D)-Gucy2e Restores Rod and Cone Function to a Mouse Model of Leber Congenital Amaurosis

Finally, we asked whether AAV44.9(E531D) containing the hGRK1 promoter, the most potent and translationally relevant capsid/promoter identified in this study, could deliver therapeutic transgene to both rods and cones and restore their function in a mouse model of IRD. To do so, we selected a mouse model lacking both rod and cone function due to the absence of any functioning retinal guanylate cyclase, the retinal guanylate cyclase-1 (GC1)/retinal guanylate cyclase-2 (GC2) double-knockout (GCdKO) mouse. The GCdKO mouse is a well-established model of Leber congenital amaurosis-1 and has been shown to be amenable to gene replacement.^{44,45} Untreated GCdKO mice have no rod- or cone-mediated electroretinogram (ERG). Treatment with AAV44.9(E531D)-hGRK1-*Gucy2e* resulted in significant recovery of both cone- and rod-mediated function, indicating efficient expression of GC1 in both cell types (Figure 8). Photopic (cone-mediated) function was restored to approximately 61% of wild-type (WT), and scotopic (rod-mediated) function was restored to approximately 28% of WT. Our previous work in this mouse model using an AAV8(Y733F)-based vector resulted in between 26% and 42% recovery of rod function, and between 29% and 44% recovery of cone function.⁴⁵ This range of values was based on treatment time points that ranged between postnatal day 18 (P18) to P108. Mice in the current study were treated between P35 and P49. While a direct comparison was not made, these data suggest that AAV44.9(E531D) may be more effective capsid for conferring therapy to cones.

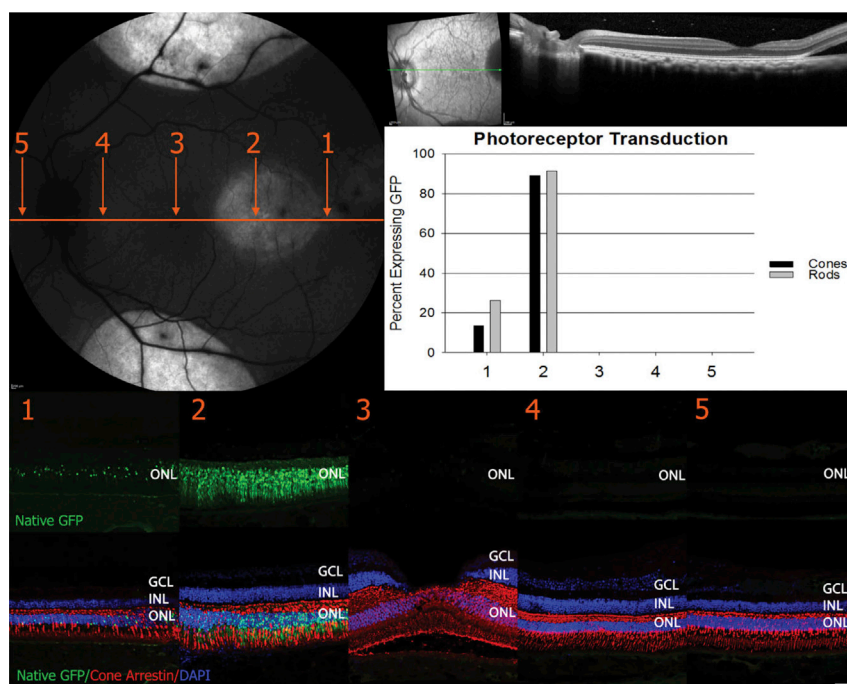


Figure 4. Retinal Transduction by AAV5-hGRK1-GFP following Extrafoveal Subretinal Injections in Macaque (1×10^{12} vg/mL)

Three 30- μ L blebs were delivered at a distance of approximately 25 degrees of eccentricity from the fovea. The OCT scan (upper right) taken immediately after the dose reveals that the fovea remained attached during surgery. Confocal scanning laser ophthalmoscopy (SLO) performed 2 weeks p.i. shows GFP expression confined to the margins of the injection blebs (top left, and Figure 3). Retinal cross-sections from the five zones demarcated in the SLO image were stained with an antibody raised against cone arrestin (red) and counterstained with DAPI (blue). Zone 3 corresponds to the foveal pit. Qualitative analysis (IHC [immunohistochemistry] of retinal cross-sections, bottom) reveals that AAV5-hGRK1-mediated GFP expression (green) is restricted predominantly to rods and cones within the bleb margins. No foveal cones were transduced in zone 3. This is supported by quantification (graph, middle right, and Table S3). Scale bar in retinal cross-sections, 40 μ m. ONL, outer nuclear layer; INL, inner nuclear layer; GCL, ganglion cell layer.

DISCUSSION

This study identifies AAV44.9 and AAV44.9(E531D) as promising AAV capsids for the treatment of retinal disease wherein photoreceptor cells are the target. We show that AAV44.9 is significantly more efficient than AAV5- and AAV8-based vectors in SRI mice. Addition of the E531D mutation further enhanced transduction efficiency, with AAV44.9(E531D) retaining tropism for both rods and cones. Of particular interest was the observation in mice that a single SRI of AAV44.9 and AAV44.9(E531D) led to transduction of the majority of photoreceptors. AAV44.9(E531D) transduced ~90% of rods in *Nrl*-GFP mice (see Figure 1). As this was not observed with AAV5 or AAV8, we posited that this resulted in part from lateral spread beyond the injection bleb margins by 44.9-based vectors. Later experiments in SRI macaques confirmed this to be true. Transgene expression mediated by 44.9-based vectors was observed well outside the bleb margins, while expression from benchmark AAV5 remained confined to the bleb, as expected.⁹

AAV44.9 and AAV44.9(E531D) transduced >95% of foveal cones and central rods following extrafoveal SRI (foveas were not detached during surgery). In fact, the percent transduction following extrafoveal injection was almost identical to that observed following direct submacular injection. Post-injection OCT scans showed no apparent structural changes to the fovea following extrafoveal SRI. In contrast, macaque retinas that received submacular injections exhibited transient loss of the ellipsoid zone and foveal bulge, both of which are consistent with retinal detachment (see Figures S12 and S13).^{42,43} This is important given reports that injection of AAV vector under the fovea of some LCA2 patients led to central retinal thinning and loss of visual acuity.⁸ Similar decreases in retinal thickness were

observed following macular SRI in NHPs⁴⁶ and, more recently, in choroideremia patients treated in clinical trials.⁴⁷ What still needs to be determined is whether the magnitude of foveal cone expression is greater when vector is placed directly under retina versus laterally spreading into this region. Related to this is how the number and placement (eccentricity from fovea) of satellite blebs influence transgene expression in foveal cones. Longitudinal in-life images illustrate that the lateral spreading of AAV44.9 and AAV44.9(E531D) vectors from the three individual blebs (superior, inferior, and mid-temporal) converged at the macula, suggesting that each contributed to transduction. This finding supports further exploration of an “intersectional” SRI approach wherein small volumes of vector are delivered to multiple, distinct extrafoveal locations, each of which contributes to foveal cone transduction. While safety and tolerability were not primary endpoints of our study, and macaques did not undergo ERG assessments, complete indirect and slit-lamp ophthalmoscopic examinations were performed regularly by a board-certified veterinary ophthalmologist experienced in preclinical assessment of subretinal AAV in macaques. There were no significant findings on the examinations to indicate that the intersectional approach would be tolerated differently than the traditional single subretinal bleb approach. Only expected post-operative effects were observed, including minimal post-operative inflammation and RPE pigment changes within the dosing site. Another advantage of lateral spreading vectors is that they may compensate for the inability to control the direction with which SRI blebs propagate, thereby mitigating the need to make adjustments to cannula placement within the retinotomy.⁴⁷ Taken together, extrafoveal SRI of these novel, laterally spreading capsids may represent a substantial advancement over the existing clinical strategies for targeting transgene expression to

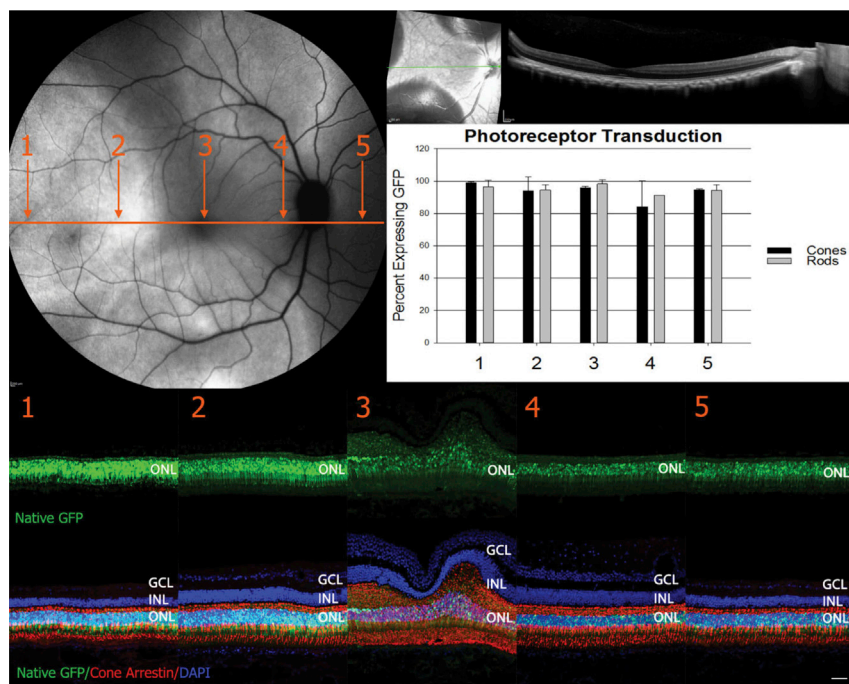


Figure 5. Retinal Transduction by AAV44.9-hGRK1-GFP following Extrafoveal Subretinal Injections in Macaque (1×10^{12} vg/mL)

Three 30- μ L blebs were delivered at a distance of approximately 25 degrees of eccentricity from the fovea. The OCT scan (upper right) taken immediately after the dose reveals that the fovea remained attached during surgery. Confocal scanning laser ophthalmoscopy (SLO) performed 2 weeks p.i. shows that GFP expression has extended beyond the margins of the injection blebs (top left, and Figure 3). Retinal cross-sections from the five zones demarcated in the SLO image were stained with an antibody raised against cone arrestin (red) and counterstained with DAPI (blue). Zone 3 corresponds to the foveal pit. Qualitative analysis (IHC [immunohistochemistry] of retinal cross-sections, bottom) reveals that AAV44.9-hGRK1-mediated GFP expression (green) is present in rods and cones across all zones. 96% of foveal cones were transduced in zone 3. This is supported by quantification (graph, middle right, and Table S3). Scale bar in retinal cross-sections, 40 μ m. ONL, outer nuclear layer; INL, inner nuclear layer; GCL, ganglion cell layer.

central retina. They may also allow for more expansive transduction in retinal diseases where the target treatment area is large (i.e., retinitis pigmentosa, choroideremia). Note that Dalkara and colleagues⁴⁸ have also explored this concept, successfully transducing foveal cones in a macaque using an AAV9 variant delivered by SRI adjacent to the fovea, indicating that the approach may be successful using other AAV capsids.

Interestingly, when directly comparing AAV44.9 and AAV44.9(E531D), we found that the latter consistently outperformed the parent capsid. In mice, photoreceptor transduction efficiency was higher for AAV44.9(E531D) in all experiments, regardless of vector concentration. In macaques, both AAV44.9 and AAV44.9(E531D) transduced photoreceptors with high efficiency. When focusing on parafoveal cones, a target cell difficult to transduce by AAV,¹³ we observed that submacular injection (i.e., parafovea contained within the injection bleb) of AAV44.9-CBA and AAV44.9-hGRK1 vectors resulted in clear transgene expression in these cells (see Figures S8 and S9). However, when the parafovea was not included in the surgical bleb, AAV44.9-hGRK1 did not drive transgene expression in parafoveal or perifoveal cones, despite robust expression in rods for each respective area. In contrast, we observed clear transgene expression in parafoveal and perifoveal cones following extrafoveal SRI of AAV44.9(E531D)-hGRK1 (see Figures S13 and 7). Additionally, when looking at the relative placement of the extrafoveal blebs for the respective retinas (see Figure 3, negative contrast images taken at day of dosing), bleb edges in the AAV44.9(E531D)-hGRK1-treated retina were generally farther away from the fovea than those in the AAV44.9-hGRK1-injected retina. We therefore

conclude that overall the performance of AAV44.9(E531D) was superior to the parent capsid. The observation of parafoveal and perifoveal cone transduction by AAV44.9 following submacular, but not extrafoveal, injection suggests that this delivery method is more effective for targeting vector to parafoveal and perifoveal cones than when virus laterally spreads into this region from a peripheral site of injection. This leads us to speculate that AAV44.9 spread outside the injection bleb may occur along or adjacent to the outer plexiform layer (OPL), and not within the subretinal interphase of photoreceptors and RPE. Transit along the OPL into the parafovea/perifovea would result in vector directly contacting rod cell bodies given their proximal location to the OPL as opposed to cone cell bodies, which are more distal to the OPL. When vector spreads farther into the fovea there are only cone cell bodies, and thus these cones are efficiently transduced. In contrast, when AAV44.9 vector is placed directly under the parafovea/perifovea, it may traffic through the outer nuclear layer (ONL), coming into contact with both cone and rod cell bodies, thus transducing both. This may also explain the apparent tropism shift away from RPE and toward photoreceptors exhibited by AAV44.9 in macaque retina. These hypotheses warrant further investigation in follow-up experiments.

What is the basis for this lateral spread by AAV44.9-based vectors? Interactions with surface molecules of the extracellular matrix (ECM) can limit biodistribution of AAVs through direct interactions with the capsid. We previously explored the interaction of AAV2-based capsids with HSPG and how this relates to retinal transduction.²⁵ Despite being recognized as a primary receptor, AAV2 variants lacking HSPG-binding residues show enhanced retinal

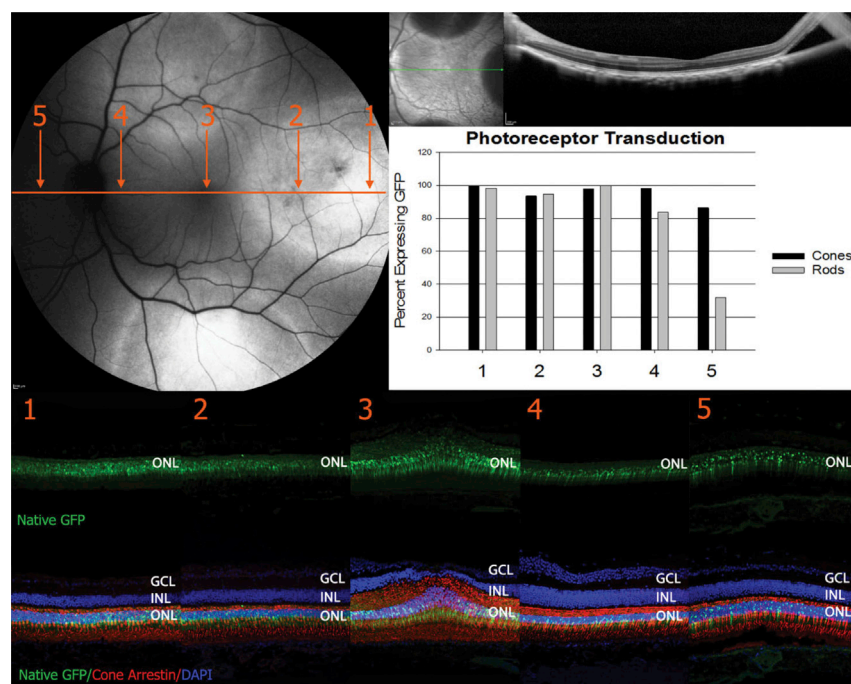


Figure 6. Retinal Transduction by AAV44.9(E531D)-hGRK1-GFP following Extrafoveal Subretinal Injections in Macaque (1×10^{12} vg/mL)

Three 30- μ L blebs were delivered at a distance of approximately 25 degrees of eccentricity from the fovea. The OCT scan (upper right) taken immediately after the dose reveals that the fovea remained attached during surgery. Confocal scanning laser ophthalmoscopy (SLO) performed 2 weeks p.i. shows that GFP expression has extended beyond the margins of the injection blebs (top left, and Figure 3). Retinal cross-sections from the five zones demarcated in the SLO image were stained with an antibody raised against cone arrestin (red) and counterstained with DAPI (blue). Zone 3 corresponds to the foveal pit. Qualitative analysis (IHC [immunohistochemistry] of retinal cross-sections, bottom) reveals that AAV44.9-hGRK1-mediated GFP expression (green) is present in rods and cones across all zones. 98% of foveal cones are transduced within the foveal pit. This is supported by quantification (graph, middle right, and Table S3). Scale bar in retinal cross-sections, 40 μ m. ONL, outer nuclear layer; INL, inner nuclear layer; GCL, ganglion cell layer.

transduction when delivered by SRI.^{12,25} They also show improved volumetric spread and transduction in the brain.^{49,50} AAV44.9 does not bind heparin, nor does the closely related AAVrh.8, which we confirmed in this study. When we grafted heparin binding onto AAV44.9 via an E531K substitution, we predictably saw a decrease in retinal transduction following SRI, a result consistent with the hypothesis that increased interaction of capsid with the ECM can limit transduction of surrounding cells. This is further supported by another study grafting HSPG binding onto AAVrh.8R.¹² As of yet, however, no study has empirically determined a relationship between ECM binding and AAV transduction in the subretinal space.

AAV5 does not bind HSPG, but it promotes transgene expression that remains confined to the margins of the subretinal bleb in macaques.⁹ Another glycan-capsid interaction, in this case with sialic acid (SIA), likely accounts for the lack of AAV5 spread. AAV5 binds to and utilizes SIA for transduction.⁵¹ SIA is abundant in the interphotoreceptor matrix and on the surface of photoreceptors.⁵² AAV44.9 shares the same capsid footprint in variable region I (VRI) with AAVrh.8 and other related capsids (e.g., AAVrh.10) that was identified to be a determinant of transport across the blood-brain barrier (BBB).^{53,54} Recent evidence suggests that this same footprint on other AAVs (such as AAV1) promotes an interaction with SIA, and that the homologous footprint for BBB-crossing capsids (such as AAVrh.8) lack this SIA interaction.⁵⁵ Current evidence points to the lack of HSPG and SIA binding as contributing factors to the lateral spread of this vector within the subretinal matrix; however, additional studies are required to identify the specific glycan-capsid interactions dictating tropism for AAV44.9, as are experiments to determine how the E531D substitution is improving

AAV44.9 transduction. Prior studies looking specifically at this substitution on AAV2 (E530D in AAV2 numbering) have found that AAV2(E530D) displays enhanced transduction *in vitro* without altering receptor interaction.⁵⁶

Neither AAV44.9 nor AAV44.9(E531D) transduced retina following IVI. A previous report showed that two closely related capsids, AAVrh.8 and AAVrh.10, transduced inner and middle retina of mice following IVI.¹⁴ However, vectors in that study were delivered at a relatively high concentration of 1.0×10^{13} vg/mL (2×10^{10} vg in 2 μ L). The authors reported variable and “patchy” transduction, and it is unclear how expansive transduction was in the images presented (i.e., how much area of retina was transduced). A more recent study evaluated transduction of AAVrh.10 in intravitreally injected mice, rats, and rabbits.⁵⁷ Again, relatively high doses were used and, in some cases, injections were performed in neonates and in models of inherited retinal degeneration, two conditions that increase transduction efficiency of intravitreally delivered vector in mice. Fundus images from all species were restricted to the region immediately surrounding the optic nerve head, and results were highly variable. Further complicating things, neither previous study incorporated a benchmark vector (AAV2) for comparison. Given the promiscuous spreading phenotype observed by AAV44.9 in our study, it is conceivable that the outer retinal transduction observed in these studies by similar vectors was associated with capsid accessing the retina through lateral spread from small areas of detached retina and/or optic nerve head, and not through the internal limiting membrane (ILM), as is the case for AAV2-based vectors. This may also explain the variability; it is common for trans-scleral IVIs or manipulation of the vitreous

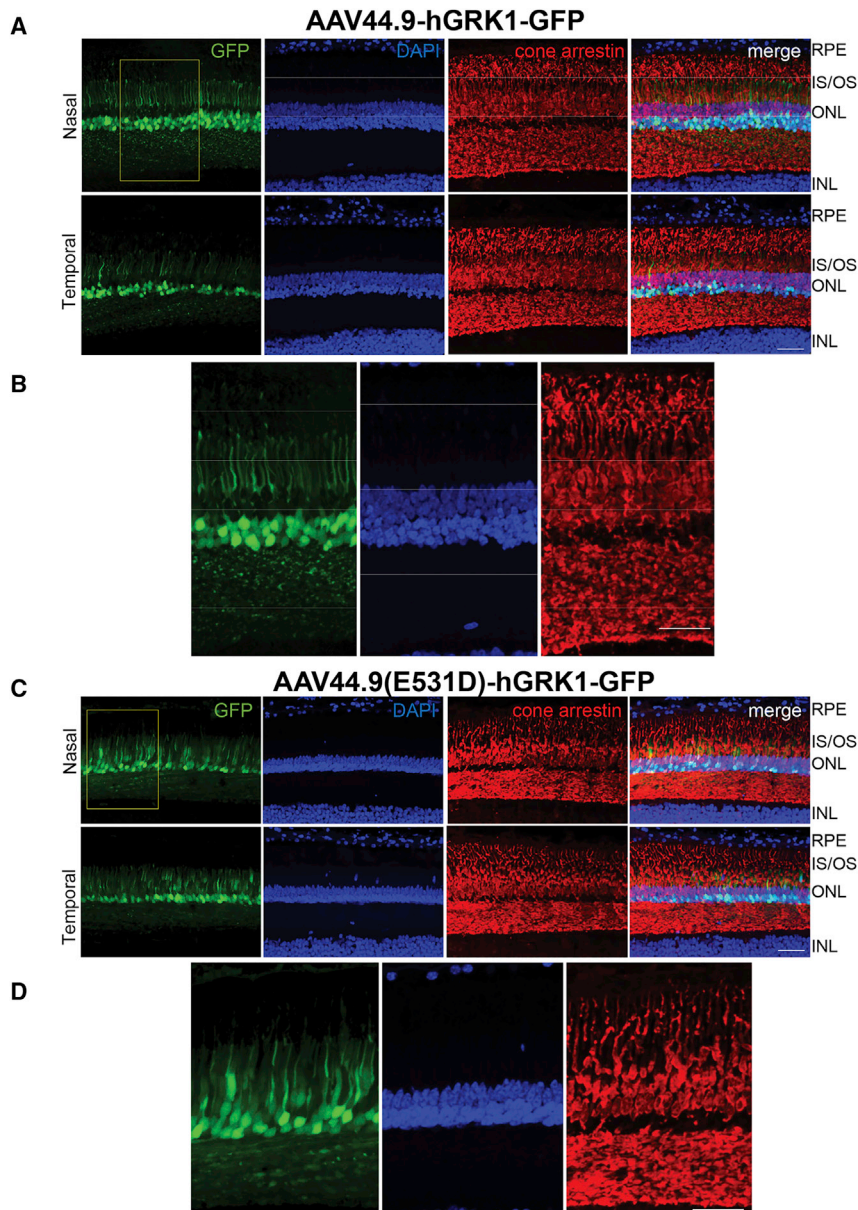


Figure 7. AAV-Mediated GFP Expression in Macaques that Received Extrafoveal Subretinal Injections

Retinal cross-sections from macaque eyes that received extrafoveal subretinal injections (SRI) of AAV44.9-hGRK1-GFP (A and B) or AAV44.9(E531D)-hGRK1-GFP (C and D) were immunostained with an antibody raised against cone arrestin (red) and counterstained with DAPI (blue). GFP expression (green) was absent from parafoveal cones (~550 μm nasal or temporal from the foveal pit) in eyes injected with AAV44.9. In contrast, parafoveal cones efficiently expressed AAV44.9(E531D)-mediated GFP. $\times 20$ original magnification (A and C) and $\times 40$ original magnification (B and D) images are shown. Scale bars in (A) and (C), 40 μm , and in (B) and (D), 20 μm . RPE, retinal pigment epithelium; IS/OS, inner segments/outer segments; ONL, outer nuclear layer; INL, inner nuclear layer.

efficacy of the candidate capsid can be directly evaluated in preclinical animal models.

Efforts to develop less invasive approaches for targeting photoreceptors (namely foveal cones) are underway, with emphasis placed on IVI because it avoids the need to detach the fovea. However, published evidence suggests that none of the novel capsid variants developed to date exhibits the efficiency of photoreceptor transduction required to confer therapy. They also require delivery doses that are bordering on toxicity (e.g., inflammation).² Our study shows that there may be an alternative and more effective strategy to address certain IRDs. AAV44.9(E531D) represents a significant refinement to the SRI technique wherein the injection bleb can be placed in a region of the retina proximal to the target area. Due to lateral spreading, therapeutic transgene expression may be achievable without perturbation of the fragile diseased region of retina or, in the case of some IRDs, disruption of the only remaining locus of functioning retina.

to result in damage to the retina that promotes access of vector into the subretinal space.⁵⁸

We observed that AAV44.9(E531D) vectored *Gucy2e* restored both cone and rod responses in GCdKO mice. While this may seem inconsequential in comparison to the data collected in primate retina, it is a major benefit when considering that successful preclinical development requires demonstration of consistent potency across AAV manufacturing lots. This can be challenging when an *in vitro* activity assay is lacking, when the candidate capsid fails to transduce cells in culture, or in cases where a tissue-specific promoter in the transgene cassette does not drive sufficient expression in available cell lines. All of these hurdles become moot when the ef-

This approach increases efficiency (photoreceptors transduced at levels expected to confer therapy), and arguably safety. Our results strongly suggest that AAV44.9(E531D) will be useful for treating diseases where the central retina is the therapeutic target, but direct detachment of the fovea is contraindicated. It could also be useful for addressing IRDs where the goal is to treat an expansive area of retina.

MATERIALS AND METHODS

AAV Capsid Phylogenetic Tree

VP1 amino acid sequences for AAVs were aligned using ClustalW (AlignX-Vector NTI). The alignment was then used to generate a phylogenetic tree via the neighbor-joining methods using the EMBL-EBI

Simple Phylogeny program (https://www.ebi.ac.uk/Tools/phylogeny/simple_phylogeny/). The resulting tree was visualized using the Tree-View program, and AAV5 was designated as the outgroup.

AAV Plasmid Construction and Vector Production

AAV rep/cap plasmid containing AAV2 rep and VP1 sequence corresponding to AAV44.9(Y733F) cap was constructed by PCR amplification of a partial AAV44.9 VP1 sequence from plasmid DNA containing the original AAV44.9 isolate clone. The AAV44.9 VP1 fragment was ligated into rep2-cap8(Y733F) plasmid in place of existing AAV8(Y733F) cap using the internal MluI site, thereby leaving the last 6 aa residues in place, including F733. The resulting plasmid AAV rep2-capAAV44.9(Y733F) was subjected to site-directed mutagenesis to create plasmids coding for AAV44.9, AAV44.9(E531K), and AAV44.9(E531D), which were confirmed by Sanger sequencing. AAVrep2-AAVrh.8 plasmid was created by PCR amplification of a partial AAVrh.8 VP1 sequence and ligated in place of AAV44.9 VP1. Plasmids for packaging AAV2, AAV5, and AAV8(Y733F) were already available and have been described previously.²⁵ Self-complementary AAV constructs containing the truncated chimeric CMV (cytomegalovirus)-chicken β -actin (smCBA) promoter driving mCherry (sc-smCBA-mCherry)⁵⁹ were packaged into AAV44.9, AAV44.9(E531D), AAV44.9(Y733F), AAV44.9(E531K), AAVrh.8, AAV8(Y733F), AAV6, AAV2, or AAV5 for use *in vitro* and in mice. Additional constructs containing the cone-specific, IRBP-GNAT2 chimeric promoter driving GFP, or the human rhodopsin kinase (hGRK1) promoter driving murine guanylate cyclase (*Gucy2e*), were packaged in AAV44.9 or AAV44.9(E531D) for use in mice.^{19,60} All vectors were packaged using a triple transfection plasmid-based system in adherent HEK293T cells seeded in double-stack cell factories (1,272-cm² cell growth area). Cells were harvested and lysed by successive freeze-thaw cycles. Virus within the lysate was purified by iodixanol density gradient and was buffer exchanged into Alcon BSS (balanced salt solution) supplemented with Tween 20 (0.014%). Virus was titered by qPCR relative to a standard and stored at -80°C . Finally, AAV constructs containing either the CBA or hGRK1 promoter driving GFP were packaged in AAV44.9, AAV44.9(E531D), or AAV5 for use in NHP experiments at a larger scale (10-stack cell factory, 6,360-cm² cell growth area). These vectors were purified as above with the addition of ion-exchange chromatography using a HiTrap Q column (GE Healthcare) according to previously published methods.¹⁷ Each undiluted vector preparation was tested for the presence of endotoxin, with all registering less than 5 endotoxin units (EU)/mL.

In Vitro Transduction Assay

ARPE-19 (human retinal pigment epithelial cell line) cells were seeded in 96-well plates at a concentration of 1.0×10^4 cells/well. The following day, cells were infected at 10,000 particles/cell. Three days post-infection, fluorescent microscopy at a fixed exposure was performed, cells were detached, and flow cytometry was used to quantify reporter protein expression (mCherry) via fluorescence. mCherry expression was calculated by multiplying the mean mCherry fluorescence times the number of positive cells, as previously described.²³

Heparin-Binding Assay

To assess the ability of AAVs to bind heparan sulfate (HS), heparin-binding profiles of AAV6, AAV5, AAVrh8, AAV44.9, and AAV44.9(E531D) were determined using affinity chromatography starting at either physiologic osmolarity (isotonic) or below physiologic osmolarity. 200 μL of heparin-agarose type I resin was loaded into Micro Bio-Spin columns (Bio-Rad, catalog #7326204) (Sigma, H6508). Columns were equilibrated with either standard PBS (phosphate-buffered saline)-MK buffer ($1 \times$ PBS, 1 mM MgCl_2 , 2.5 mM KCl [pH 7.4]) with an estimated osmolarity of 310 mOsm or “low”-MK buffer ($2/3 \times$ PBS, 1 mM MgCl_2 , 2.5 mM KCl [pH 7.4]) with an estimated osmolarity of 210 mOsm. Columns were then washed with 1 mL of either MK or low-MK supplemented with 1 M NaCl and two additional 1-mL MK or low-MK washes. Samples were formulated to contain 600 ng of virus in 500- μL total volume in MK or low-MK buffer. 250 μL was set aside to act as a loading control, and the other 250 μL was loaded onto the column and the flow-through was collected by gravity. The columns then underwent five 1-mL washes with MK or low-MK buffer, and eleven 1.5-mL elutions under conditions of increasing concentrations of NaCl, ranging from 50 mM to 1 M (50–500 mM, 1 M NaCl in MK or low-MK). Following sample collection and elution, samples were heat-denatured (boiled at 99°C for 10 min) and visualized by B1 dot blot. The B1 monoclonal antibody (mAb) primary antibody (American Research Products, catalog #03-65158; 1:3,000 in LI-COR Biosciences Odyssey blocking buffer, 0.2% Tween 20) was used to detect a linear epitope at the C-terminal end of the AAV VP3 common region.⁶¹ The samples were visualized using a donkey anti-mouse IR-Dye 680RD secondary antibodies (LI-COR Biosciences, catalog #926-68072) and imaged using the LI-COR Biosciences Odyssey CLX system.

Animal Ethics Statement

All mice were bred and maintained at the University of Florida Health Science Center Animal Care Services Facility under a 12-h light/12-h dark cycle. Food and water were available *ad libitum*. All experiments were approved by the University of Florida’s Institutional Animal Care and Use Committee and were conducted in accordance with the ARVO (The Association for Research in Vision and Ophthalmology) Statement for the Use of Animals in Ophthalmic and Vision Research and within National Institutes of Health regulations. Seven adult male macaques (*M. fascicularis*) were used in this study. All procedures performed on the macaques were approved by Institutional Animal Care and Use Committees at Charles River Laboratories and performed in accordance with the Association for Research in Vision and Ophthalmology Statement for the Use of Animals in Ophthalmic and Vision Research.

Mouse Injections

One microliter of vector at concentrations of 2×10^{12} vg/mL (high dose) or 2×10^{11} vg/mL (low dose) was delivered either intravitreally or subretinally to 4- to 5-week-old *Nrl*-GFP and C57BL/6J mice. One microliter of AAV44.9(E531D)-hGRK1-*Gucy2e* or AAV8(Y733F)-hGRK1-*Gucy2e* was delivered subretinally to 5- to 7-week-old GCdKO mice at a concentration of 1×10^{13} vg/mL. All injections were

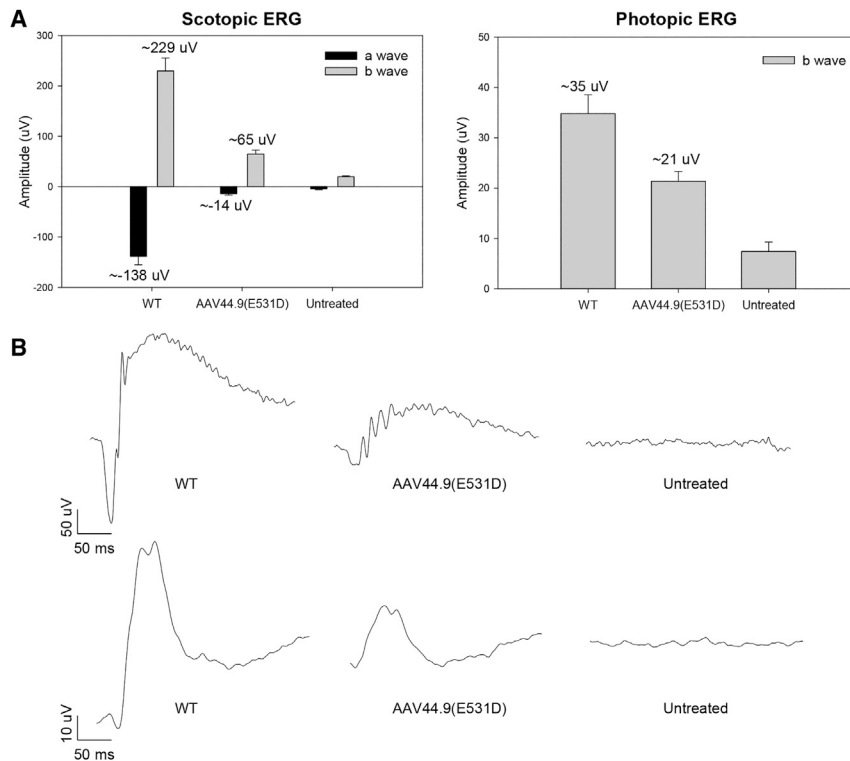


Figure 8. Subretinally Delivered AAV44.9(E531D)-hGRK1-Gucy2e (1×10^{13} vg/mL) Restores Retinal Function to the GCdKO Mouse Model of Leber Congenital Amaurosis (LCA1)

GCdKO ($n = 8$) mice received SRI of $1 \mu\text{L}$ of vector in one eye only. Contralateral control eyes remained uninjected. At each time point, maximum scotopic and photopic b-wave amplitudes (those generated at 0 and 10 dB, respectively) from all injected and un-injected (contralateral) eyes, as well as age-matched C57BL/6J controls ($n = 12$), were averaged as mean \pm SEM. Unpaired, two-tailed Student's *t* tests were used, and significance = $p < 0.05$. At 4 weeks post-injection, significant improvements were observed in the scotopic (rod-mediated) a- and b-wave amplitudes and photopic (cone-mediated) b-wave amplitudes in treated eyes. Amplitudes in uninjected control eyes were unchanged (at the level of "noise"). Average maximum amplitudes are plotted in (A), and representative traces (scotopic, top; photopic, bottom) are shown in (B).

Measurement of Retinal Transduction via Flow Cytometry

Methods for assessing transduction of mouse retina have been described previously.²⁵ Briefly, neural retinas (i.e., RPE manually stripped from retina) from between four and six Nrl-GFP eyes per cohort were harvested and dissociated with papain. Flow cytometry was performed on treated, dissociated retinas and untreated controls to quantify the percentage of cells that were positive for GFP (i.e., rod photoreceptors), mCherry (non-rod retinal neurons transduced by rAAV), or both (rod photoreceptors transduced by rAAV). The percentages of rods and non-rod neural retinal cells transduced by each vector were separately averaged. Kruskal-Wallis tests were performed, followed by a *post hoc* Dunn's test to make pairwise comparisons between groups. For the non-rod values, $H = 44.912$, degrees of freedom (df) = 6, and $p < 0.001$. For the rod values, $H = 85.546$, df = 6, and $p < 0.001$.

performed under a Leica M80 stereomicroscope according to previously published methods.⁶² A minimum of six eyes receiving successful injections were analyzed in each experiment. Injection blebs were imaged immediately following injection, and further analysis was carried out only on animals that received comparable successful injections ($\geq 60\%$ retinal detachment and minimal complications).

Macaque Injections

Seven cynomolgus macaques received SRI of either AAV44.9, AAV44.9(E531D), or AAV5 vectors containing either the CBA or hGRK1 promoter driving GFP, each at a concentration of 1×10^{12} vg/mL. In four animals, two $60\text{-}\mu\text{L}$ injections were performed (one intentionally submacular, and one peripheral). In three animals, three $30\text{-}\mu\text{L}$ extrafoveal injections were performed at a distance of approximately 25 degrees of eccentricity from the fovea. Superior and inferior blebs were made along the vertical meridian immediately adjacent to the venule within the vascular arcades when possible. Temporal injections were made along the horizontal meridian either immediately superior or inferior to the temporal nerve fiber raphe.

In-Life Imaging

At 4 weeks p.i., funduscopy was performed on mice using a Micron III camera (Phoenix Research Laboratories, Pleasanton, CA, USA). Bright-field and red fluorescent images were taken to visualize retinal health and mCherry expression, respectively. Exposure settings remained constant between experiments. OCT and confocal scanning laser ophthalmoscopy (cSLO) were performed on injected macaques pre-injection, immediately p.i., and at 1, 2, 4, and 6 weeks p.i.

Tissue Preparation and Immunostaining

Four weeks p.i., mice were humanely sacrificed, and their eyes were enucleated and fixed overnight at 4°C in freshly prepared 4% paraformaldehyde (PFA) in PBS. Cornea and lens were removed, and the eye cup was incubated in 30% sucrose solution overnight at 4°C . Eyes were embedded in cryostat compound and frozen at -80°C . Sections ($12 \mu\text{m}$ thick) were cut using a cryostat (Leica Microsystems, Buffalo Grove, IL, USA) and transferred to glass slides. Retinal cryosections were rinsed with $1 \times$ PBS, blocked with 0.5% Triton X-100 and 1% bovine serum albumin (BSA) for 1 h each, and then incubated overnight at 4°C with mouse monoclonal anti-cone arrestin antibody (1:1,000, generously provided by Dr. Clay Smith). The following day slides were rinsed with $1 \times$ PBS and then incubated at room temperature for 1 h with Alexa Fluor donkey anti-mouse secondary antibody (1:500) in $1 \times$ PBS and counterstained with DAPI. Images were acquired using a confocal laser scanning microscope (Leica TCS SP8) and a fluorescence microscope (EVOS). Six weeks p.i., macaques were

humanely sacrificed and their eyes enucleated and processed as previously described.⁹ Retinal sections were stained with an antibody directed against cone arrestin, counterstained with DAPI, and imaged using identical settings with a laser scanning confocal microscope (Leica TCS SP8).

Quantification of GFP-Positive Cone and Rod Photoreceptors at Different Locations within the Macaque Retina

Three blinded observers counted the number of GFP-positive cones and rods in macaque retinal cross-sections that were stained with DAPI to identify individual photoreceptor cells within the outer nuclear layer, and a cone-specific antibody (cone arrestin) to identify cones versus rods. Any native GFP signal within the outer nuclear layer above background signal present from the inner nuclear layer, that co-labeled with DAPI, was interpreted as a GFP-positive photoreceptor. Images used for counting were captured at equal settings (laser power, gain) with a laser scanning confocal microscope (Leica TCS SP8). In some retinas, percentages were quantified in five discrete retinal regions across a single plane traversing the foveal pit (temporal to nasal). Distances for each region from the center of the optic nerve head were (approximately) as follows: region 1, 8,580 μm ; region 2, 5,720 μm ; region 3, 2,860 μm ; region 4, 800 μm ; region 5 1,600 μm nasal to the optic nerve head.

Electroretinogram (ERG)

ERGs were recorded using a fully integrated Celeris system (Diagnosys, Lowell, MA, USA). Following overnight dark adaptation, scotopic (rod-mediated) ERGs were elicited at intensities ranging from -20 to 0 dB with interstimulus intervals of 30 s, averaged from five measurements at each intensity. Mice were then light-adapted to a 30 cd/m^2 white background for 5 min. Photopic (cone-mediated) responses were elicited with intensities ranging from -3 dB to 10 dB. Fifty responses with interstimulus intervals of 0.4 s were recorded in the presence of a 20 cd/m^2 white background and averaged at each intensity. At each time point, maximum scotopic and photopic b-wave amplitudes (those generated at 0 and 10 dB, respectively) from all injected and un-injected (contralateral) eyes were averaged as mean \pm SEM. An unpaired two-tailed Student's *t* test was used to compare these samples.

SUPPLEMENTAL INFORMATION

Supplemental Information can be found online at <https://doi.org/10.1016/j.ymthe.2020.04.002>.

AUTHOR CONTRIBUTIONS

S.E.B., S.L.B., and J.A.C. participated in the conception of the project and design of experiments. S.E.B. and S.L.B. wrote the paper and secured funding. S. Choudhury, S. Crosson, R.M., J.P., K.R.C., D.F., H.Z., and R.F.B. performed experiments. R.F.B. contributed to figure generation. S. Crosson, J.A.C., G.D.P., and S.A. provided reagents, feedback, and edited the manuscript. All authors provided input on the final manuscript.

CONFLICTS OF INTEREST

The authors declare no competing interests.

ACKNOWLEDGMENTS

This study was supported by an NEI grant to S.E.B. (R01 EY024280), and by an NIDCR NIH intramural research grant to J.A.C. (1ZIAD000695).

REFERENCES

- Constable, I.J., Lai, C.M., Magno, A.L., French, M.A., Barone, S.B., Schwartz, S.D., Blumenkranz, M.S., Degli-Esposti, M.A., and Rakoczy, E.P. (2017). Gene therapy in neovascular age-related macular degeneration: three-year follow-up of a phase 1 randomized dose escalation trial. *Am. J. Ophthalmol.* *177*, 150–158.
- Heier, J.S., Kherani, S., Desai, S., Dugel, P., Kaushal, S., Cheng, S.H., Delacono, C., Purvis, A., Richards, S., Le-Halpere, A., et al. (2017). Intravitreal injection of AAV2-sFLT01 in patients with advanced neovascular age-related macular degeneration: a phase 1, open-label trial. *Lancet* *390*, 50–61.
- Cukras, C., Wiley, H.E., Jeffrey, B.G., Sen, H.N., Turriff, A., Zeng, Y., Vijayarath, C., Marangoni, D., Ziccardi, L., Kjellstrom, S., et al. (2018). Retinal AAV8-RS1 gene therapy for X-linked retinoschisis: initial findings from a phase I/IIa trial by intravitreal delivery. *Mol. Ther.* *26*, 2282–2294.
- Kotterman, M.A., Yin, L., Strazzeri, J.M., Flannery, J.G., Merigan, W.H., and Schaffer, D.V. (2015). Antibody neutralization poses a barrier to intravitreal adeno-associated viral vector gene delivery to non-human primates. *Gene Ther.* *22*, 116–126.
- Yin, L., Greenberg, K., Hunter, J.J., Dalkara, D., Kolstad, K.D., Masella, B.D., Wolfe, R., Visel, M., Stone, D., Libby, R.T., et al. (2011). Intravitreal injection of AAV2 transduces macaque inner retina. *Invest. Ophthalmol. Vis. Sci.* *52*, 2775–2783.
- Dalkara, D., Byrne, L.C., Klimczak, R.R., Visel, M., Yin, L., Merigan, W.H., Flannery, J.G., and Schaffer, D.V. (2013). In vivo-directed evolution of a new adeno-associated virus for therapeutic outer retinal gene delivery from the vitreous. *Sci. Transl. Med.* *5*, 189ra76.
- Mingozzi, F., and High, K.A. (2013). Immune responses to AAV vectors: overcoming barriers to successful gene therapy. *Blood* *122*, 23–36.
- Jacobson, S.G., Cideciyan, A.V., Ratnakaram, R., Heon, E., Schwartz, S.B., Roman, A.J., Peden, M.C., Aleman, T.S., Boye, S.L., Sumaroka, A., et al. (2012). Gene therapy for Leber congenital amaurosis caused by *RPE65* mutations: safety and efficacy in 15 children and adults followed up to 3 years. *Arch. Ophthalmol.* *130*, 9–24.
- Boye, S.E., Alexander, J.J., Boye, S.L., Witherspoon, C.D., Sandefer, K.J., Conlon, T.J., Erger, K., Sun, J., Ryals, R., Chiodo, V.A., et al. (2012). The human rhodopsin kinase promoter in an AAV5 vector confers rod- and cone-specific expression in the primate retina. *Hum. Gene Ther.* *23*, 1101–1115.
- Bruewer, A.R., Mowat, F.M., Bartoe, J.T., Boye, S.L., Hauswirth, W.W., and Petersen-Jones, S.M. (2013). Evaluation of lateral spread of transgene expression following subretinal AAV-mediated gene delivery in dogs. *PLoS ONE* *8*, e60218.
- Vandenbergh, L.H., Breous, E., Nam, H.J., Gao, G., Xiao, R., Sandhu, A., Johnston, J., Debyser, Z., Agbandje-McKenna, M., and Wilson, J.M. (2009). Naturally occurring singleton residues in AAV capsid impact vector performance and illustrate structural constraints. *Gene Ther.* *16*, 1416–1428.
- Sullivan, J.A., Stanek, L.M., Lukason, M.J., Bu, J., Osmond, S.R., Barry, E.A., O'Riordan, C.R., Shihabuddin, L.S., Cheng, S.H., and Scaria, A. (2018). Rationally designed AAV2 and AAVrh8R capsids provide improved transduction in the retina and brain. *Gene Ther.* *25*, 205–219.
- Vandenbergh, L.H., Bell, P., Maguire, A.M., Xiao, R., Hopkins, T.B., Grant, R., Bennett, J., and Wilson, J.M. (2013). AAV9 targets cone photoreceptors in the nonhuman primate retina. *PLoS ONE* *8*, e53463.
- Giove, T.J., Sena-Esteves, M., and Eldred, W.D. (2010). Transduction of the inner mouse retina using AAVrh8 and AAVrh10 via intravitreal injection. *Exp. Eye Res.* *91*, 652–659.
- Halder, S., Van Vliet, K., Smith, J.K., Duong, T.T., McKenna, R., Wilson, J.M., and Agbandje-McKenna, M. (2015). Structure of neurotropic adeno-associated virus AAVrh8. *J. Struct. Biol.* *192*, 21–36.

16. Gao, G., Vandenberghe, L.H., Alvira, M.R., Lu, Y., Calcedo, R., Zhou, X., and Wilson, J.M. (2004). Clades of adeno-associated viruses are widely disseminated in human tissues. *J. Virol.* 78, 6381–6388.
17. Zolotukhin, S., Potter, M., Zolotukhin, I., Sakai, Y., Loiler, S., Fraites, T.J., Jr., Chiodo, V.A., Phillipsberg, T., Muzyczka, N., Hauswirth, W.W., et al. (2002). Production and purification of serotype 1, 2, and 5 recombinant adeno-associated viral vectors. *Methods* 28, 158–167.
18. Khabou, H., Cordeau, C., Pacot, L., Fisson, S., and Dalkara, D. (2018). Dosage thresholds and influence of transgene cassette in adeno-associated virus-related toxicity. *Hum. Gene Ther.* 29, 1235–1241.
19. Dyka, F.M., Boye, S.L., Ryals, R.C., Chiodo, V.A., Boye, S.E., and Hauswirth, W.W. (2014). Cone specific promoter for use in gene therapy of retinal degenerative diseases. *Adv. Exp. Med. Biol.* 801, 695–701.
20. Petrs-Silva, H., Dinculescu, A., Li, Q., Min, S.H., Chiodo, V., Pang, J.J., Zhong, L., Zolotukhin, S., Srivastava, A., Lewin, A.S., and Hauswirth, W.W. (2009). High-efficiency transduction of the mouse retina by tyrosine-mutant AAV serotype vectors. *Mol. Ther.* 17, 463–471.
21. Pang, J.J., Dai, X., Boye, S.E., Barone, I., Boye, S.L., Mao, S., Everhart, D., Dinculescu, A., Liu, L., Umino, Y., et al. (2011). Long-term retinal function and structure rescue using capsid mutant AAV8 vector in the *rd10* mouse, a model of recessive retinitis pigmentosa. *Mol. Ther.* 19, 234–242.
22. Dalkara, D., Byrne, L.C., Lee, T., Hoffmann, N.V., Schaffer, D.V., and Flannery, J.G. (2012). Enhanced gene delivery to the neonatal retina through systemic administration of tyrosine-mutated AAV9. *Gene Ther.* 19, 176–181.
23. Ryals, R.C., Boye, S.L., Dinculescu, A., Hauswirth, W.W., and Boye, S.E. (2011). Quantifying transduction efficiencies of unmodified and tyrosine capsid mutant AAV vectors in vitro using two ocular cell lines. *Mol. Vis.* 17, 1090–1102.
24. Ellis, B.L., Hirsch, M.L., Barker, J.C., Connelly, J.P., Steininger, R.J., 3rd, and Porteus, M.H. (2013). A survey of ex vivo/in vitro transduction efficiency of mammalian primary cells and cell lines with Nine natural adeno-associated virus (AAV1-9) and one engineered adeno-associated virus serotype. *Virol. J.* 10, 74.
25. Boye, S.L., Bennett, A., Scalabrino, M.L., McCullough, K.T., Van Vliet, K., Choudhury, S., Ruan, Q., Peterson, J., Agbandje-McKenna, M., and Boye, S.E. (2016). Impact of heparan sulfate binding on transduction of retina by recombinant adeno-associated virus vectors. *J. Virol.* 90, 4215–4231.
26. Woodard, K.T., Liang, K.J., Bennett, W.C., and Samulski, R.J. (2016). Heparan sulfate binding promotes accumulation of intravitreally delivered adeno-associated viral vectors at the retina for enhanced transduction but weakly influences tropism. *J. Virol.* 90, 9878–9888.
27. Dalkara, D., Kolstad, K.D., Caporale, N., Visel, M., Klimczak, R.R., Schaffer, D.V., and Flannery, J.G. (2009). Inner limiting membrane barriers to AAV-mediated retinal transduction from the vitreous. *Mol. Ther.* 17, 2096–2102.
28. Xie, Q., Lerch, T.F., Meyer, N.L., and Chapman, M.S. (2011). Structure-function analysis of receptor-binding in adeno-associated virus serotype 6 (AAV-6). *Virology* 420, 10–19.
29. Wu, Z., Asokan, A., Grieger, J.C., Govindasamy, L., Agbandje-McKenna, M., and Samulski, R.J. (2006). Single amino acid changes can influence titer, heparin binding, and tissue tropism in different adeno-associated virus serotypes. *J. Virol.* 80, 11393–11397.
30. Curcio, C.A. (2001). Photoreceptor topography in ageing and age-related maculopathy. *Eye (Lond.)* 15, 376–383.
31. Curcio, C.A., Medeiros, N.E., and Millican, C.L. (1996). Photoreceptor loss in aged-related macular degeneration. *Invest. Ophthalmol. Vis. Sci.* 37, 1236–1249.
32. Goto-Omoto, S., Hayashi, T., Gekka, T., Kubo, A., Takeuchi, T., and Kitahara, K. (2006). Compound heterozygous *CNGA3* mutations (R436W, L633P) in a Japanese patient with congenital achromatopsia. *Vis. Neurosci.* 23, 395–402.
33. Owsley, C., Jackson, G.R., Cideciyan, A.V., Huang, Y., Fine, S.L., Ho, A.C., Maguire, M.G., Lolley, V., and Jacobson, S.G. (2000). Psychophysical evidence for rod vulnerability in age-related macular degeneration. *Invest. Ophthalmol. Vis. Sci.* 41, 267–273.
34. Robson, A.G., Egan, C.A., Luong, V.A., Bird, A.C., Holder, G.E., and Fitzke, F.W. (2004). Comparison of fundus autofluorescence with photopic and scotopic fine-matrix mapping in patients with retinitis pigmentosa and normal visual acuity. *Invest. Ophthalmol. Vis. Sci.* 45, 4119–4125.
35. Cideciyan, A.V., Swider, M., Aleman, T.S., Feuer, W.J., Schwartz, S.B., Russell, R.C., Steinberg, J.D., Stone, E.M., and Jacobson, S.G. (2012). Macular function in macular degenerations: repeatability of microperimetry as a potential outcome measure for ABCA4-associated retinopathy trials. *Invest. Ophthalmol. Vis. Sci.* 53, 841–852.
36. Mackay, D.S., Ocaka, L.A., Borman, A.D., Sergouniotis, P.I., Henderson, R.H., Moradi, P., Robson, A.G., Thompson, D.A., Webster, A.R., and Moore, A.T. (2011). Screening of *SPATA7* in patients with Leber congenital amaurosis and severe childhood-onset retinal dystrophy reveals disease-causing mutations. *Invest. Ophthalmol. Vis. Sci.* 52, 3032–3038.
37. Okano, K., Maeda, A., Chen, Y., Chauhan, V., Tang, J., Palczewska, G., Sakai, T., Tsuneoka, H., Palczewski, K., and Maeda, T. (2012). Retinal cone and rod photoreceptor cells exhibit differential susceptibility to light-induced damage. *J. Neurochem.* 121, 146–156.
38. Robson, A.G., Michaelides, M., Luong, V.A., Holder, G.E., Bird, A.C., Webster, A.R., Moore, A.T., and Fitzke, F.W. (2008). Functional correlates of fundus autofluorescence abnormalities in patients with *RPGR* or *RIMS1* mutations causing cone or cone rod dystrophy. *Br. J. Ophthalmol.* 92, 95–102.
39. Robson, A.G., Michaelides, M., Saihan, Z., Bird, A.C., Webster, A.R., Moore, A.T., Fitzke, F.W., and Holder, G.E. (2008). Functional characteristics of patients with retinal dystrophy that manifest abnormal parafoveal annuli of high density fundus autofluorescence; a review and update. *Doc. Ophthalmol.* 116, 79–89.
40. Scholl, H.P., Chong, N.H., Robson, A.G., Holder, G.E., Moore, A.T., and Bird, A.C. (2004). Fundus autofluorescence in patients with Leber congenital amaurosis. *Invest. Ophthalmol. Vis. Sci.* 45, 2747–2752.
41. Vandenberghe, L.H., Bell, P., Maguire, A.M., Cearley, C.N., Xiao, R., Calcedo, R., Wang, L., Castle, M.J., Maguire, A.C., Grant, R., et al. (2011). Dosage thresholds for AAV2 and AAV8 photoreceptor gene therapy in monkey. *Sci. Transl. Med.* 3, 88ra54.
42. dell’Omo, R., Viggiano, D., Giorgio, D., Filippelli, M., Di Iorio, R., Calò, R., Cardone, M., Rinaldi, M., dell’Omo, E., and Costagliola, C. (2015). Restoration of foveal thickness and architecture after macula-off retinal detachment repair. *Invest. Ophthalmol. Vis. Sci.* 56, 1040–1050.
43. Ochakovski, G.A., Peters, T., Michalakakis, S., Wilhelm, B., Wissinger, B., Biel, M., Bartz-Schmidt, K.U., and Fischer, M.D.; RD-CURE Consortium (2017). Subretinal injection for gene therapy does not cause clinically significant outer nuclear layer thinning in normal primate foveae. *Invest. Ophthalmol. Vis. Sci.* 58, 4155–4160.
44. Karan, S., Frederick, J.M., and Baehr, W. (2010). Novel functions of photoreceptor guanylate cyclases revealed by targeted deletion. *Mol. Cell. Biochem.* 334, 141–155.
45. Boye, S.L., Peshenko, I.V., Huang, W.C., Min, S.H., McDoom, I., Kay, C.N., Liu, X., Dyka, F.M., Foster, T.C., Umino, Y., et al. (2013). AAV-mediated gene therapy in the guanylate cyclase (RetGC1/RetGC2) double knockout mouse model of Leber congenital amaurosis. *Hum. Gene Ther.* 24, 189–202.
46. Jacobson, S.G., Acland, G.M., Aguirre, G.D., Aleman, T.S., Schwartz, S.B., Cideciyan, A.V., Zeiss, C.J., Komaromy, A.M., Kaushal, S., Roman, A.J., et al. (2006). Safety of recombinant adeno-associated virus type 2-*RPE65* vector delivered by ocular subretinal injection. *Mol. Ther.* 13, 1074–1084.
47. Xue, K., Groppe, M., Salvetti, A.P., and MacLaren, R.E. (2017). Technique of retinal gene therapy: delivery of viral vector into the subretinal space. *Eye (Lond.)* 31, 1308–1316.
48. Khabou, H., Garita-Hernandez, M., Chaffiol, A., Reichman, S., Jaillard, C., Brazhnikova, E., Bertin, S., Forster, V., Desrosiers, M., Winckler, C., et al. (2018). Noninvasive gene delivery to foveal cones for vision restoration. *JCI Insight* 3, 96029.
49. Kanaan, N.M., Sellnow, R.C., Boye, S.L., Coberly, B., Bennett, A., Agbandje-McKenna, M., Sortwell, C.E., Hauswirth, W.W., Boye, S.E., and Manfredsson, F.P. (2017). Rationally engineered AAV capsids improve transduction and volumetric spread in the CNS. *Mol. Ther. Nucleic Acids* 8, 184–197.
50. Naidoo, J., Stanek, L.M., Ohno, K., Trewman, S., Samaranch, L., Hadacek, P., O’Riordan, C., Sullivan, J., San Sebastian, W., Bringas, J.R., et al. (2018). Extensive transduction and enhanced spread of a modified AAV2 capsid in the non-human primate CNS. *Mol. Ther.* 26, 2418–2430.

51. Walters, R.W., Yi, S.M., Keshavjee, S., Brown, K.E., Welsh, M.J., Chiorini, J.A., and Zabner, J. (2001). Binding of adeno-associated virus type 5 to 2,3-linked sialic acid is required for gene transfer. *J. Biol. Chem.* 276, 20610–20616.
52. Bishop, P.N., Boulton, M., McLeod, D., and Stoddart, R.W. (1993). Glycan localization within the human interphotoreceptor matrix and photoreceptor inner and outer segments. *Glycobiology* 3, 403–412.
53. Yang, B., Li, S., Wang, H., Guo, Y., Gessler, D.J., Cao, C., Su, Q., Kramer, J., Zhong, L., Ahmed, S.S., et al. (2014). Global CNS transduction of adult mice by intravenously delivered rAAVrh.8 and rAAVrh.10 and nonhuman primates by rAAVrh.10. *Mol. Ther.* 22, 1299–1309.
54. Albright, B.H., Storey, C.M., Murlidharan, G., Castellanos Rivera, R.M., Berry, G.E., Madigan, V.J., and Asokan, A. (2018). Mapping the structural determinants required for AAVrh.10 transport across the blood-brain barrier. *Mol. Ther.* 26, 510–523.
55. Albright, B.H., Simon, K.E., Pillai, M., Devlin, G.W., and Asokan, A. (2019). Modulation of sialic acid dependence influences the central nervous system transduction profile of adeno-associated viruses. *J. Virol.* 93, e00332-19.
56. Lochrie, M.A., Tatsuno, G.P., Christie, B., McDonnell, J.W., Zhou, S., Surosky, R., Pierce, G.F., and Colosi, P. (2006). Mutations on the external surfaces of adeno-associated virus type 2 capsids that affect transduction and neutralization. *J. Virol.* 80, 821–834.
57. Zeng, Y., Qian, H., Wu, Z., Marangoni, D., Sieving, P.A., and Bush, R.A. (2019). AAVrh-10 transduces outer retinal cells in rodents and rabbits following intravitreal administration. *Gene Ther.* 26, 386–398.
58. Da Costa, R., Röger, C., Segelken, J., Barben, M., Grimm, C., and Neidhardt, J. (2016). A novel method combining vitreous aspiration and intravitreal AAV2/8 injection results in retina-wide transduction in adult mice. *Invest. Ophthalmol. Vis. Sci.* 57, 5326–5334.
59. Haire, S.E., Pang, J., Boye, S.L., Sokal, I., Craft, C.M., Palczewski, K., Hauswirth, W.W., and Semple-Rowland, S.L. (2006). Light-driven cone arrestin translocation in cones of postnatal guanylate cyclase-1 knockout mouse retina treated with AAV-GC1. *Invest. Ophthalmol. Vis. Sci.* 47, 3745–3753.
60. Beltran, W.A., Boye, S.L., Boye, S.E., Chiodo, V.A., Lewin, A.S., Hauswirth, W.W., and Aguirre, G.D. (2010). rAAV2/5 gene-targeting to rods:dose-dependent efficiency and complications associated with different promoters. *Gene Ther.* 17, 1162–1174.
61. Wobus, C.E., Hügler-Dörr, B., Girod, A., Petersen, G., Hallek, M., and Kleinschmidt, J.A. (2000). Monoclonal antibodies against the adeno-associated virus type 2 (AAV-2) capsid: epitope mapping and identification of capsid domains involved in AAV-2-cell interaction and neutralization of AAV-2 infection. *J. Virol.* 74, 9281–9293.
62. Timmers, A.M., Zhang, H., Squitieri, A., and Gonzalez-Pola, C. (2001). Subretinal injections in rodent eyes: effects on electrophysiology and histology of rat retina. *Mol. Vis.* 7, 131–137.

Supplemental Information

Novel AAV44.9-Based Vectors Display Exceptional Characteristics for Retinal Gene Therapy

Sanford L. Boye, Shreyasi Choudhury, Sean Crosson, Giovanni Di Pasquale, Sandra Afione, Russell Mellen, Victoria Makal, Kaitlyn R. Calabro, Diego Fajardo, James Peterson, Hangning Zhang, Matthew T. Leahy, Colin K. Jennings, John A. Chiorini, Ryan F. Boyd, and Shannon E. Boye

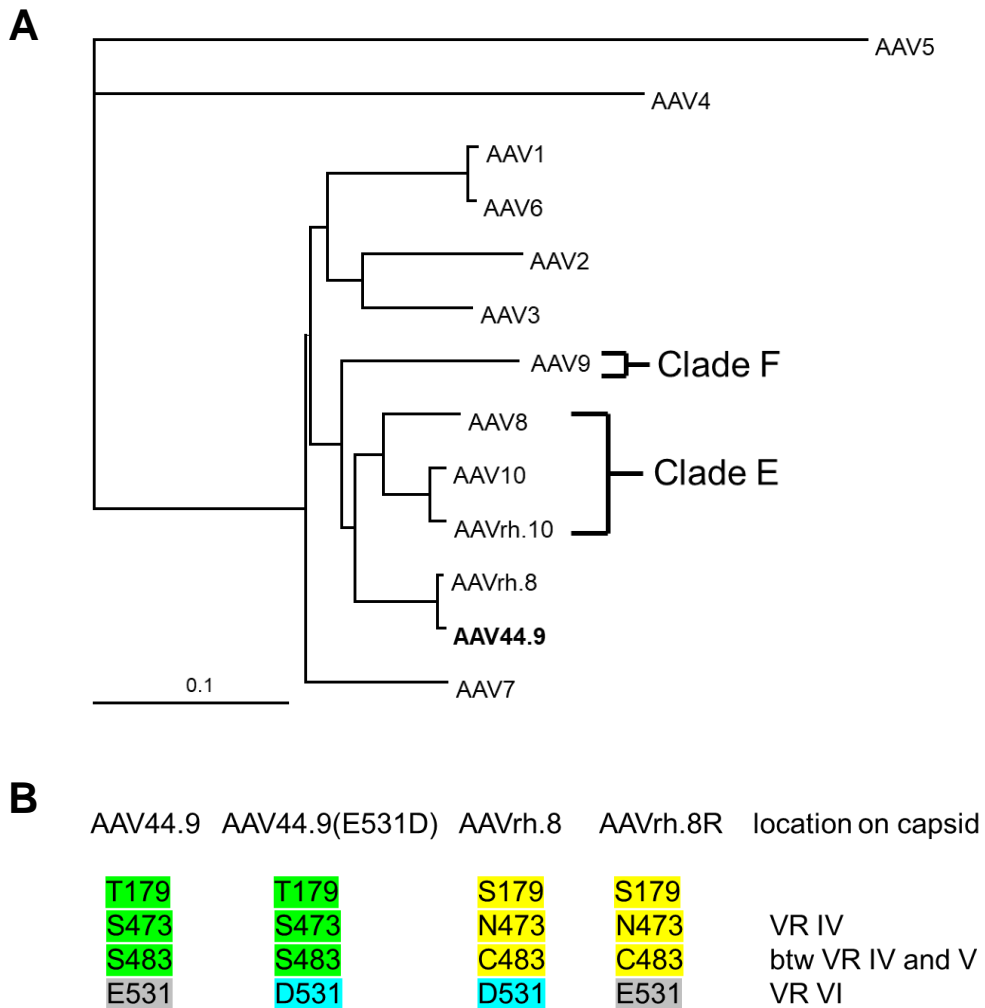


Figure S1. Phylogeny of select AAVs based on VP1 amino acid sequences using neighbor-joining method (A). Specific amino acid substitutions for AAV44.9 and related variants and location on capsid (B). Color denotes residue is shared across different capsids. VR denotes variable loop on capsid surface, IV, V and VI are roman numerals.

Vector Prep	Scale (cell surface area)	Vector Concentration (vg/mL)	Total Vector Yield (vg)	Yield/cell (vg/cell)
scAAV44.9-smCBA-mCherry	1272 cm ²	2.16E+13	2.81E+12	1.41E+04
scAAV44.9-smCBA-mCherry	1272 cm ²	1.59E+13	2.07E+12	1.04E+04
scAAV44.9(E531D)-smCBA-mCherry	1272 cm ²	1.51E+13	1.96E+12	9.80E+03
scAAV44.9(E531D)-smCBA-mCherry	1272 cm ²	1.06E+13	1.38E+12	6.90E+03
scAAV44.9(E531K)-smCBA-mCherry	1272 cm ²	5.15E+13	1.03E+13	5.15E+04
scAAV44.9(Y733F)-smCBA-mCherry	1272 cm ²	1.90E+13	2.47E+12	1.24E+04
scAAV8(Y733F)-smCBA-mCherry	1272 cm ²	2.59E+12	3.24E+11	1.62E+03
scAAVrh.8-smCBA-mCherry	1272 cm ²	1.98E+13	2.57E+12	1.29E+04
scAAV6-smCBA-mCherry	1272 cm ²	2.99E+12	4.63E+11	2.32E+03
scAAV5-smCBA-mCherry	1272 cm ²	3.82E+13	4.01E+12	2.01E+04
AAV44.9-CBA-GFP	6,360 cm ²	1.41E+13	4.23E+12	4.23E+03
AAV44.9-hGRK1-GFP	6,360 cm ²	1.49E+13	4.47E+12	4.47E+03
AAV44.9(E531D)-hGRK1-GFP	6,360 cm ²	1.60E+13	4.80E+12	4.80E+03
AAV5-hGRK1-GFP	6,360 cm ²	7.63E+12	4.12E+12	4.12E+03
AAV44.9(E531D)-hGRK1-Gucy2e	6,360 cm ²	1.17E+13	4.39E+12	4.39E+03

Table S1. Total yield and concentration of vectors produced via plasmid-based triple transfection. AAV preparations made at the 6,360cm² scale underwent additional step of ion-exchange chromatography purification.

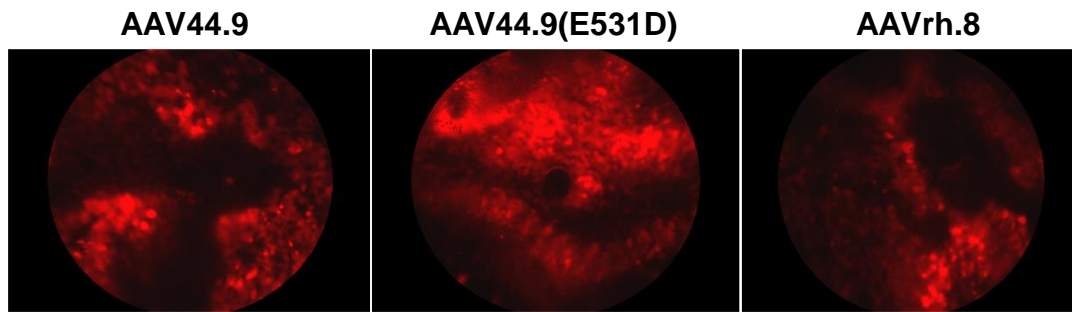


Figure S2. Qualitative analysis of retinal transduction following subretinal injection (SRI) of novel capsid variants. Representative fluorescent fundus images of Nrl-GFP mouse retinas 4 weeks post-SRI with 2×10^8 vgs of AAV44.9, AAV44.9(E531D), or AAVrh.8 vectors containing smCBA-mCherry. Images were captured using identical settings. At this lower dose, AAV44.9(E531D) outperforms both AAV44.9 and AAVrh.8.

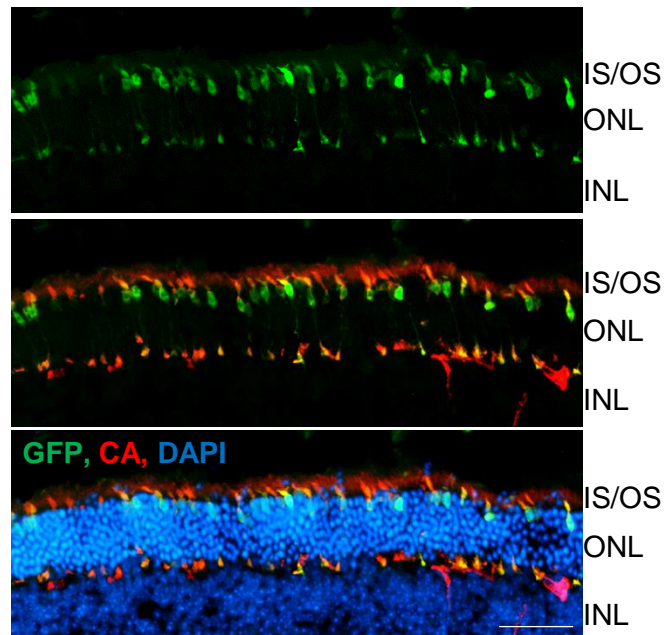


Figure S3. Transduction profile of AAV44.9-IRBP/GNAT2-GFP following SRI in C57BL6J mice. Six weeks post-injection with 2×10^{12} vg/mL, retinal cross sections were stained with an antibody directed against cone arrestin (CA) and counterstained with DAPI. Vector-mediated GFP expression and cone arrestin colocalize indicating this capsid efficiently transduces cone photoreceptors. Scale bar= 50 microns. IS/OS- inner segments/outer segments, ONL- outer nuclear layer, INL- inner nuclear layer.

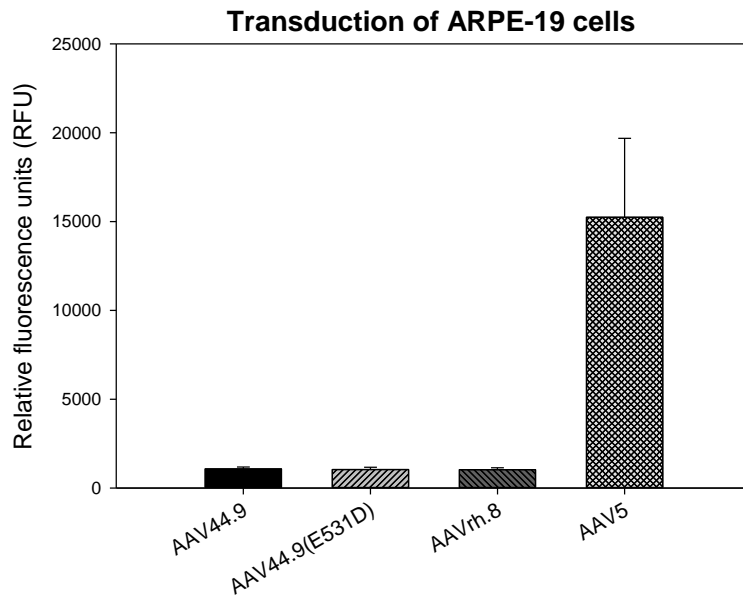


Figure S4. Quantitative analysis of transduction by novel capsid variants *in vitro*. Self-complimentary constructs containing the smCBA promoter driving mCherry were packaged in AAV44.9, AAV44.9(E531D), AAVrh.8, or AAV5. ARPE19 cells were infected with vector at an MOI of 10,000. Three days post-infection, cells were dissociated and flow cytometry used to quantify the relative fluorescence (% mCherry positive cells x fluorescence intensity).

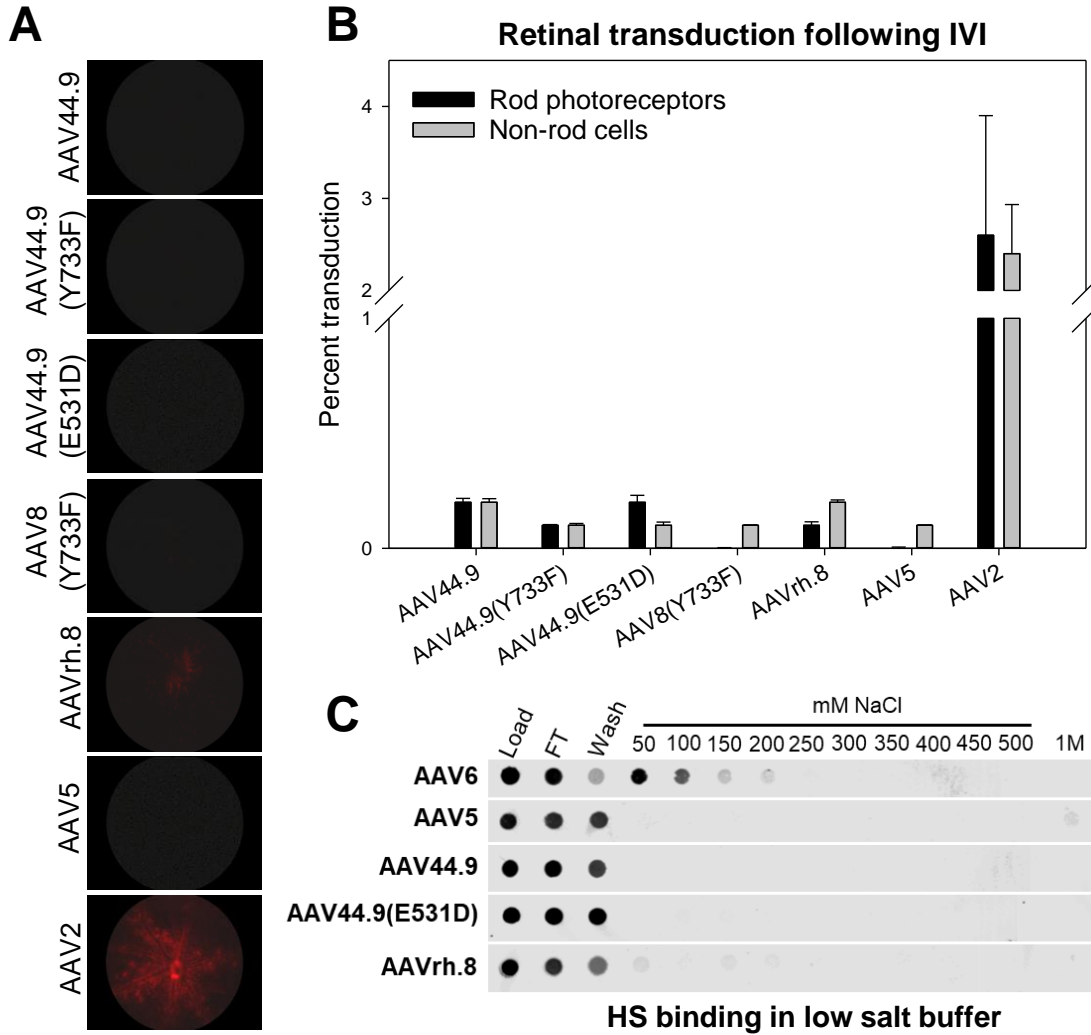


Figure S5. Qualitative (A) and quantitative (B) analysis of retinal transduction following intravitreal injection (IVI) of novel capsid variants. Fundus images of Nrl-GFP mouse retinas 4 weeks post-IVI with 2×10^9 vg of AAV44.9, AAV44.9(Y733F), AAV44.9(E531D), AAVrh.8, AAV8(Y733F), AAV5 or AAV2 (A). Images were captured using identical settings. Similar to benchmark vectors, AAV5 and AAV8(Y733F), AAV44.9 and its derivatives do not efficiently transduce retina following IVI. A closely related capsid, AAVrh.8 also fails to efficiently transduce retina via this route. Flow cytometry was performed on dissociated retinas and the percent rod vs. non-rod retinal transduction by capsids was quantified (B). Heparin binding elution profiles of AAV44.9 and AAV44.9(E531D) capsids relative to AAV6, AAV5 and AAVrh.8 at different salt concentrations (C). Background buffer was lowered to 220mOsm. Salt concentrations presented are in addition to this osmolarity.

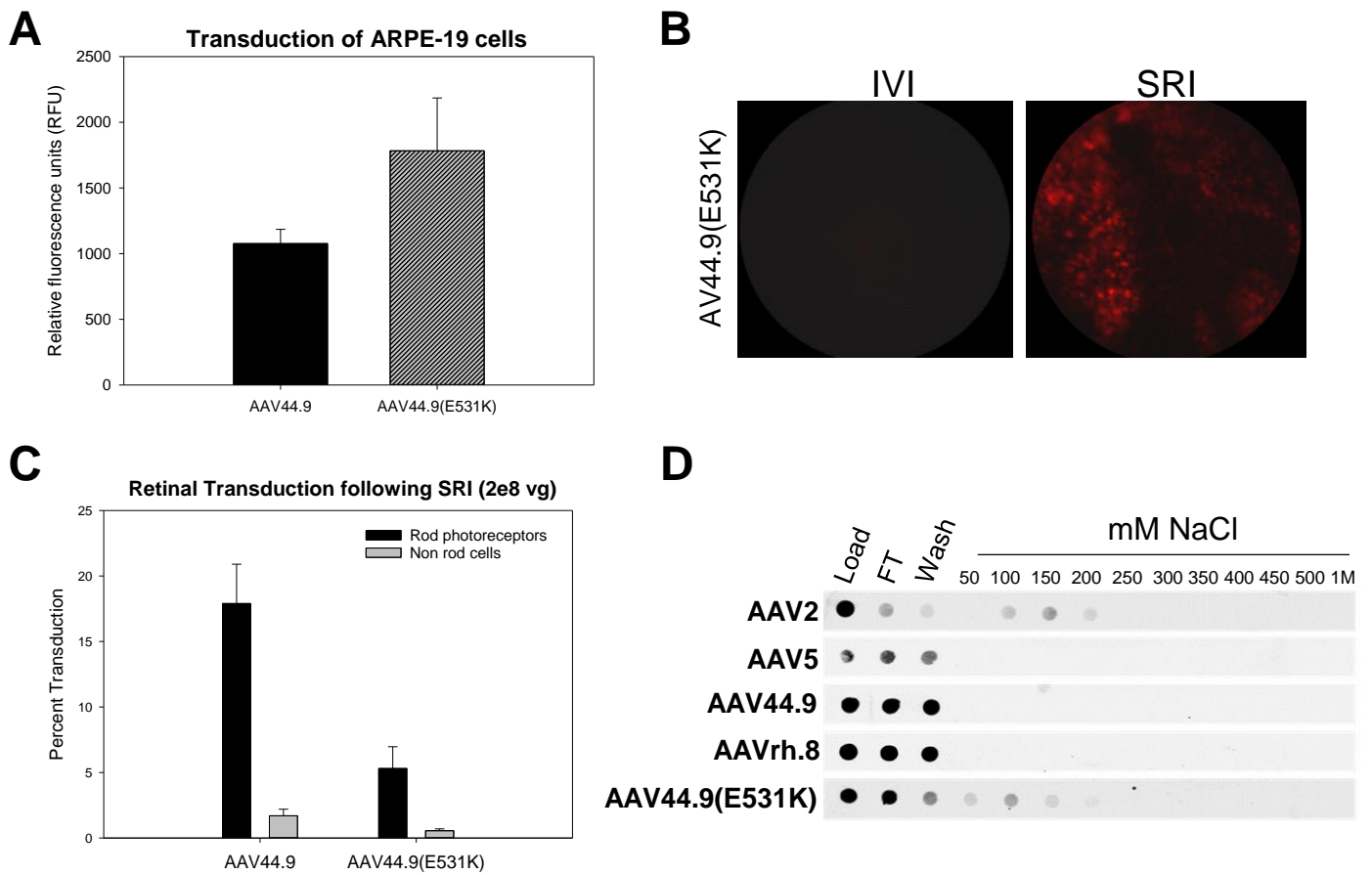


Figure S6. Quantitative analysis of transduction by AAV44.9(E531K) *in vitro*. Self-complementary constructs containing the smCBA promoter driving mCherry were packaged in AAV44.9(E531K), closely related capsids and benchmark AAV5. ARPE19 cells were infected at an MOI of 10,000. Three days post-infection, cells were dissociated and flow cytometry used to quantify relative fluorescence (% mCherry positive cells x fluorescence intensity). Qualitative (B) and quantitative (C) analysis of retinal transduction by AAV44.9(E531K) *in vivo*. Fundus images of Nrl-GFP mouse retinas 4 weeks post-IVI or SRI with 2e8 vgs of AAV44.9(E531K) (B). Images were captured using identical settings. AAV44.9(E531K) does not transduce retina following IVI and only modestly transduces retina following SRI. Flow cytometry was performed on dissociated retinas from subretinally injected mice and the percent rod vs. non-rod retinal transduction by capsids was quantified relative to closely related capsids (C). Heparin binding elution profiles of AAV44.9 and AAV44.9(E531K) capsids relative to AAV2, AAV5 and AAVrh.8 at different salt concentrations (D).

Group #	N	OD	OS	Concentration	Volume/Bleb Location
1	2	n/a	AAV44.9-CBA-GFP	1x10 ¹² vg/mL	60uL/bleb Bleb #1- submacular, Bleb #2- inferior
2	2	n/a	AAV44.9-hGRK1-GFP	1x10 ¹² vg/mL	60uL/bleb Bleb #1- submacular, Bleb #2- inferior
3	1	n/a	AAV5-hGRK1-GFP	1x10 ¹² vg/mL	90 µl, Three 30uL extrafoveal blebs
4	1	n/a	AAV44.9-hGRK1-GFP	1x10 ¹² vg/mL	90 µl, Three 30uL extrafoveal blebs
5	1	AAV44.9-hGRK1-GFP	AAV44.9(E531D)-hGRK1-GFP	1x10 ¹² vg/mL	90 µl, Three 30uL extrafoveal blebs

Table S2. NHP injection details

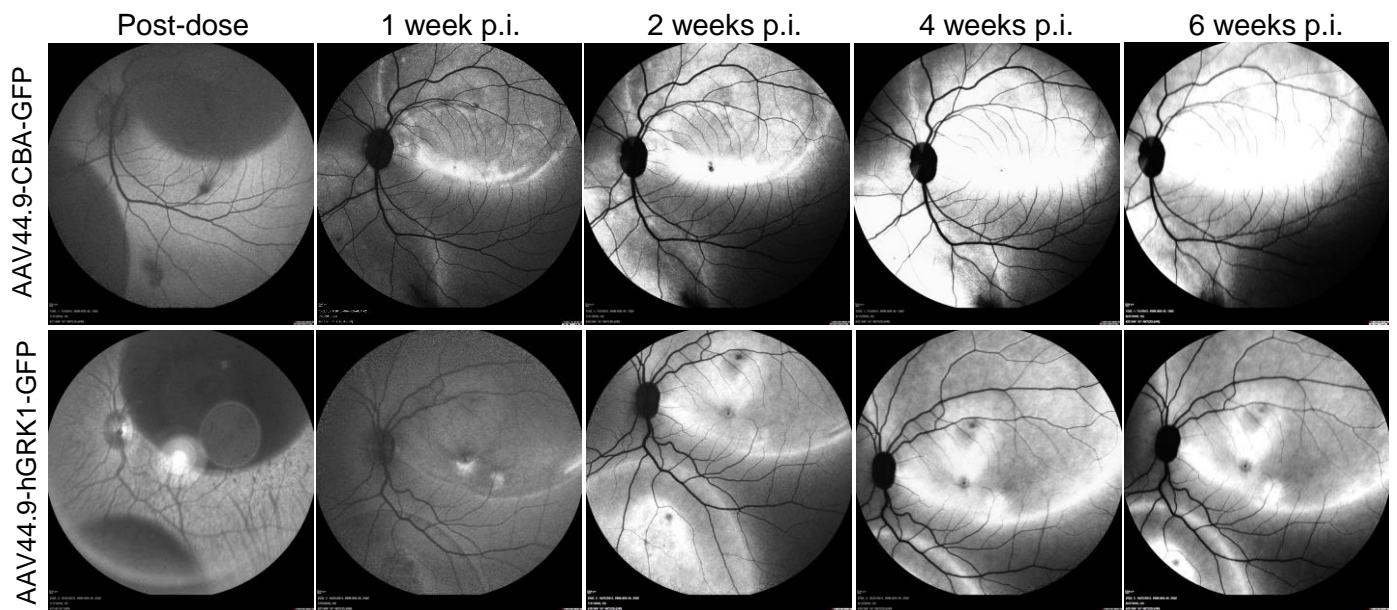
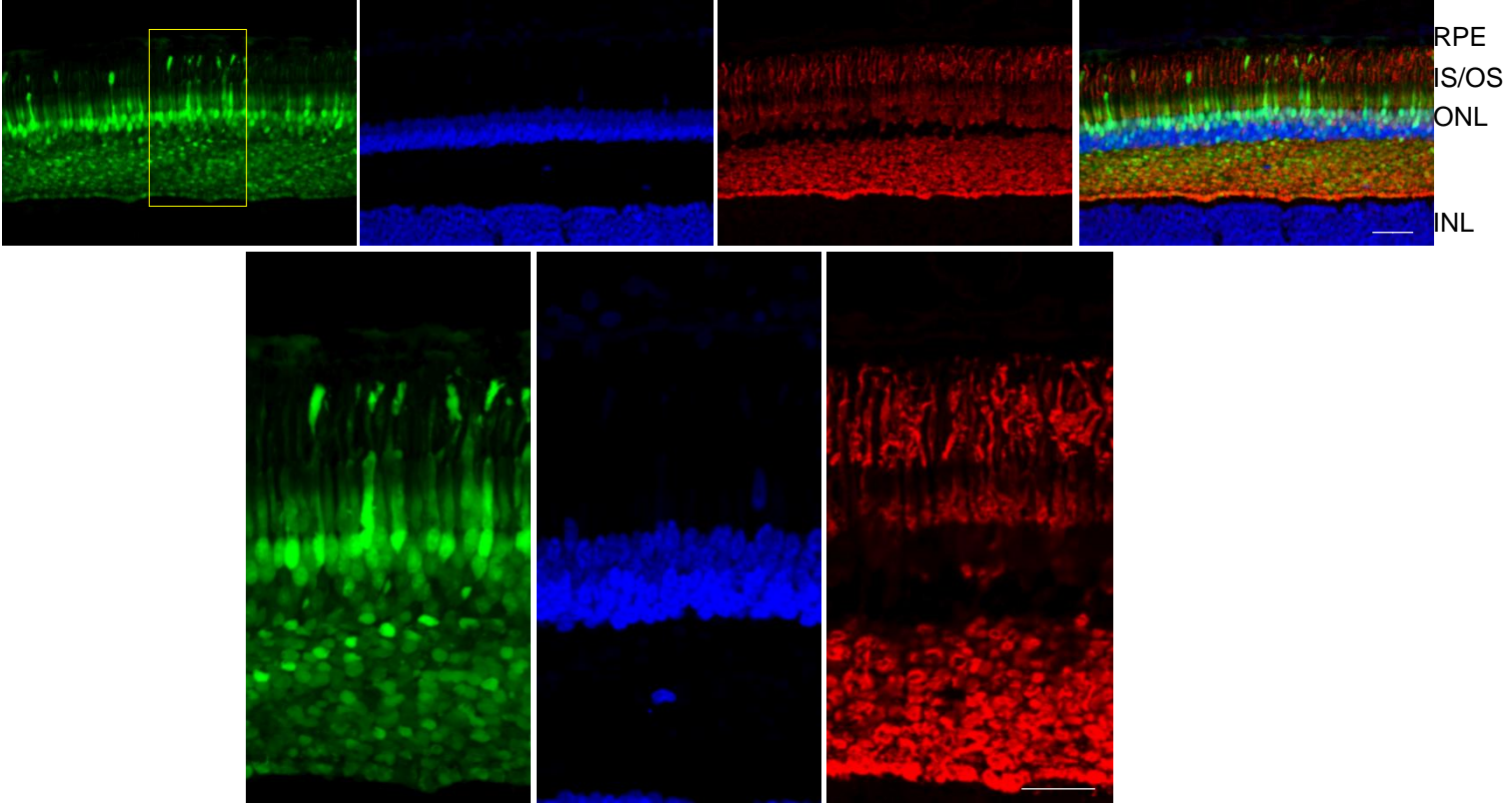


Figure S7. Representative macaque fundus images taken immediately after central and peripheral subretinal injection, then at 1 week, 2 weeks, 4 weeks and 6 weeks post-injection with either AAV44.9-CBA or AAV44.9-hGRK1 vectors driving GFP.

Vector	Bleb Location	Area Analyzed	% cones transduced	% rods transduced
AAV44.9-CBA	submacular	fovea	95%	96%
	peripheral	inferotemporal	100%	95%
AAV44.9-hGRK1	submacular	fovea	97%	81%
	peripheral	temporal	97%	96%
	extrafoveal	fovea	96%	98%
AAV44.9(E531D)-hGRK1	peripheral	temporal	93%	95%
	extrafoveal	fovea	98%	100%
AAV5-hGRK1	peripheral	temporal	89%	92%
	extrafoveal	fovea	0%	0%

Table S3. Summary of cone and rod transduction in subretinally injected macaque, according to bleb location

AAV44.9-CBA-GFP temporal parafovea



AAV44.9-CBA-GFP nasal parafovea

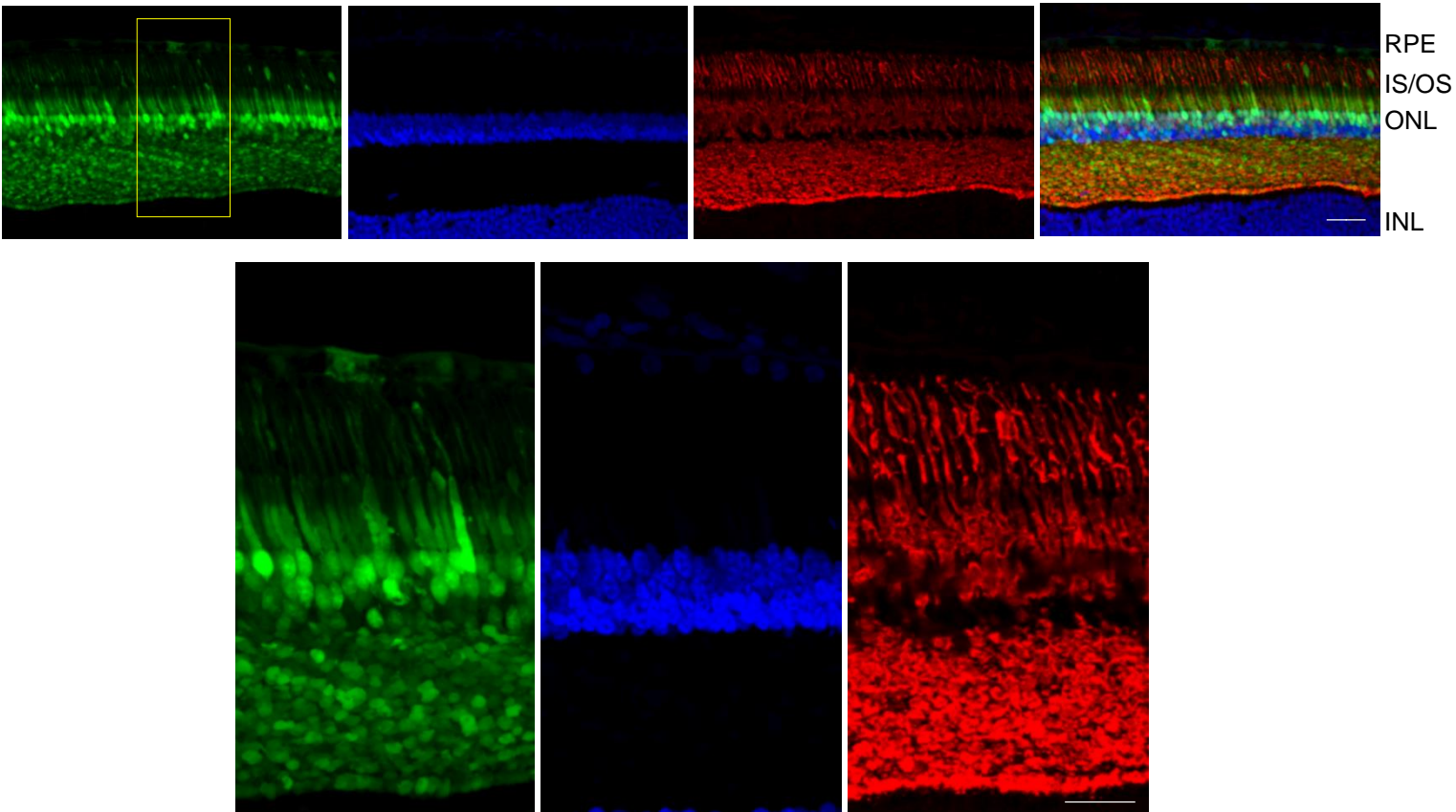


Figure S8. Representative retinal cross sections from the temporal (top) and nasal (bottom) parafovea of eyes that received submacular subretinal injection of AAV44.9-CBA-GFP. Retinas were stained with an antibody raised against cone arrestin (red) and counterstained with DAPI (blue). Scale bars in low mag (20X) images = 40 microns, high mag (40X) images= 20 microns

AAV44.9-hGRK1-GFP

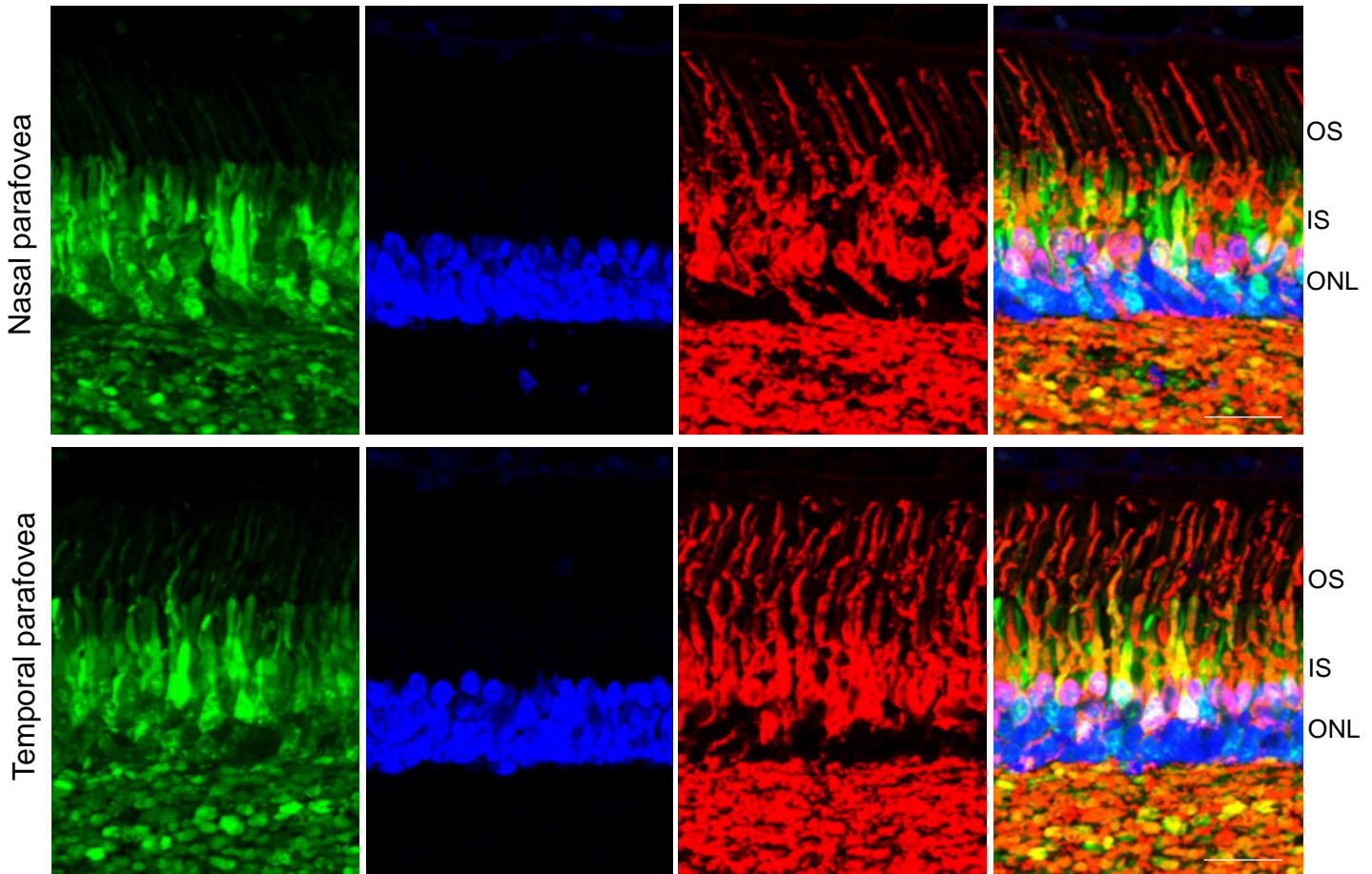


Figure S9. Retinal cross sections from macaque eyes that received submacular subretinal injections (SRI) of AAV44.9-hGRK1-GFP. Sections from the nasal and temporal parafovea were immunostained with an antibody raised against cone arrestin (red) and counter stained with DAPI (blue). GFP expression (green) was present in parafoveal cones (~550 μ M nasal or temporal from the foveal pit) in eyes injected with AAV44.9-hGRK1. Scale bars= 20 microns. IS- inner segments, OS-outer segments, ONL- outer nuclear layer

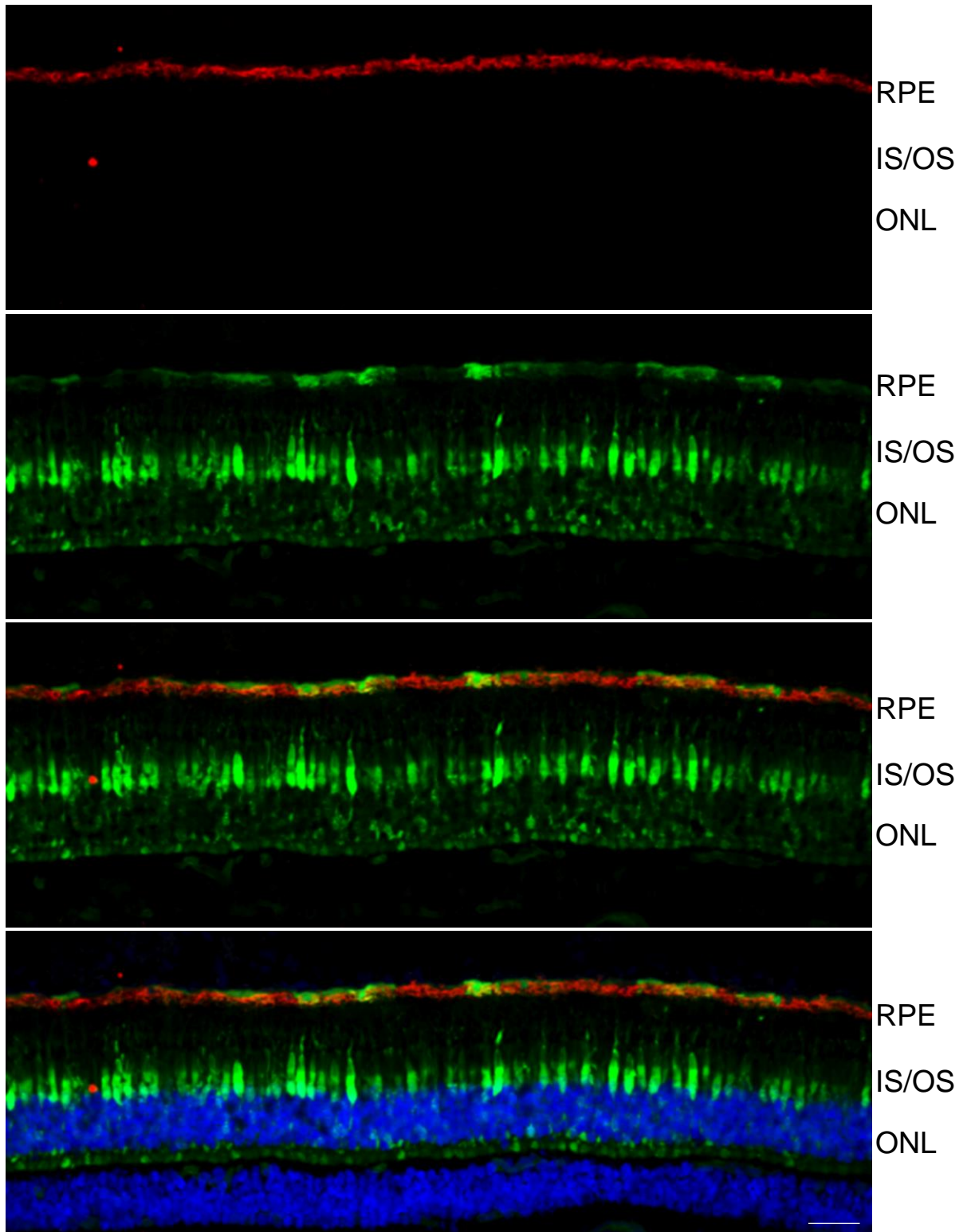


Figure S10. Representative retinal cross section from macaque eye that received subretinal injections (SRI) of AAV44.9-CBA-GFP immunostained with an antibody raised against RPE65 (red) and counter stained with DAPI (blue). 40X image is shown. Scale bar= 40 microns. RPE= retinal pigment epithelium, IS/OS= inner segments/outer segments, ONL= outer nuclear layer. Scale bar= 40 microns

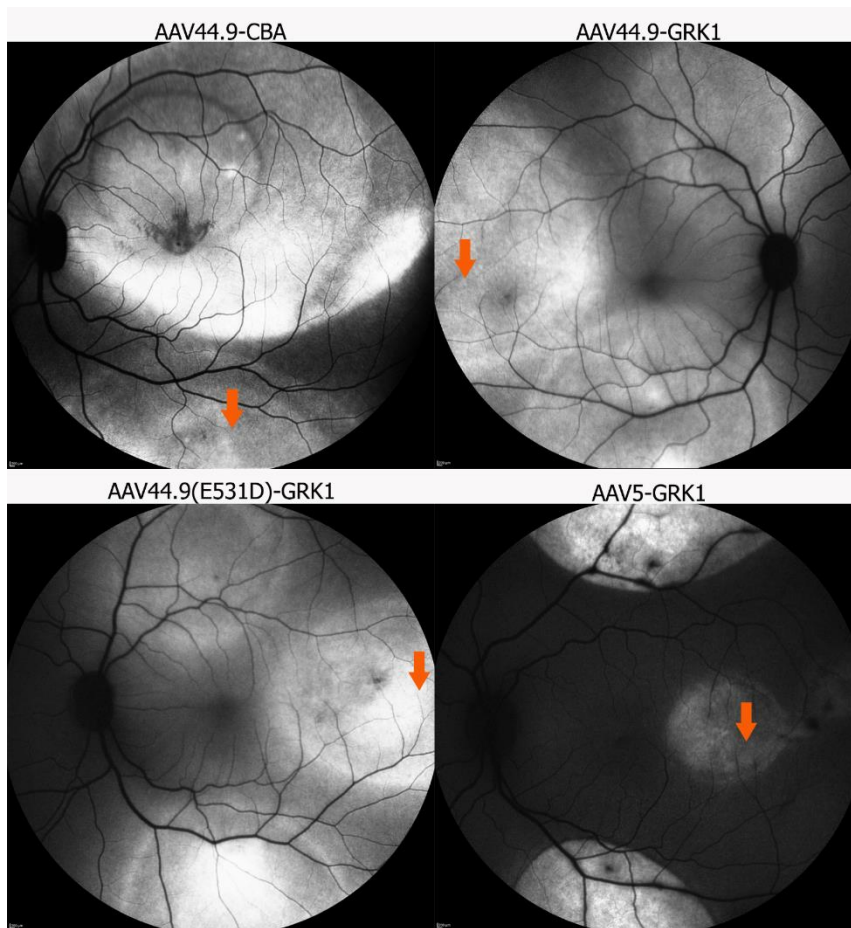


Figure S11. Confocal scanning laser ophthalmoscopy (SLO) images of macaque eyes subretinally injected with AAV44.9-CBA, AAV44.9-hGRK1, AAV44.9(E531D)-hGRK1, or AAV5-hGRK1 vectors. Orange arrows demarcate the locations in peripheral retinas from which cross sectional analyses in Figure 2 was performed.

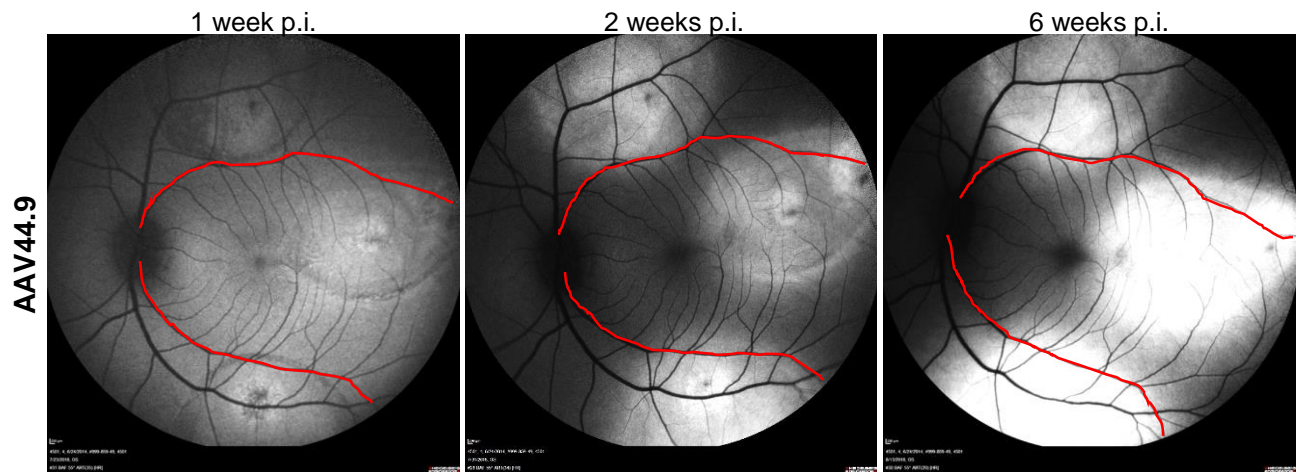


Figure S12. Confocal scanning laser ophthalmoscopy (SLO) images of macaque eyes that received 3 extrafoveal subretinal injections (30 μ L each) of AAV44.9 vector containing hGRK1-GFP (1×10^{12} vg/mL). Each injection was placed approximately 25 degrees away from the foveal pit. Images could not be obtained on the day of dosing, but were captured at 1, 2, and 6 weeks post-injection. Red lines are superimposed on retinal vasculature to serve as landmarks.

AAV44.9-hGRK1-GFP

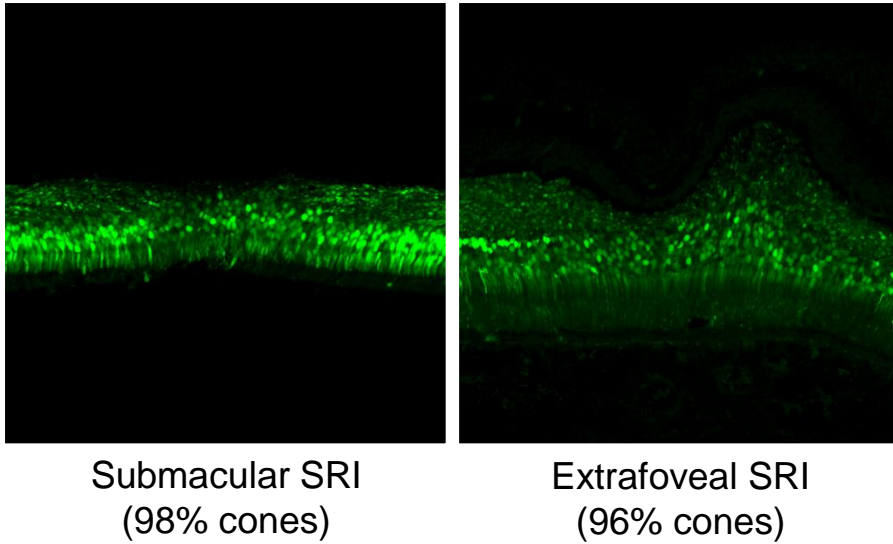


Figure S13. Photoreceptor transduction in the foveal pit of eyes that received either submacular or extrafoveal subretinal injection (SRI) of AAV44.9-hGRK1-GFP. The percent of GFP positive cones in these retinal cross sections, quantified by three blinded observers, was almost identical despite differences in surgical delivery.

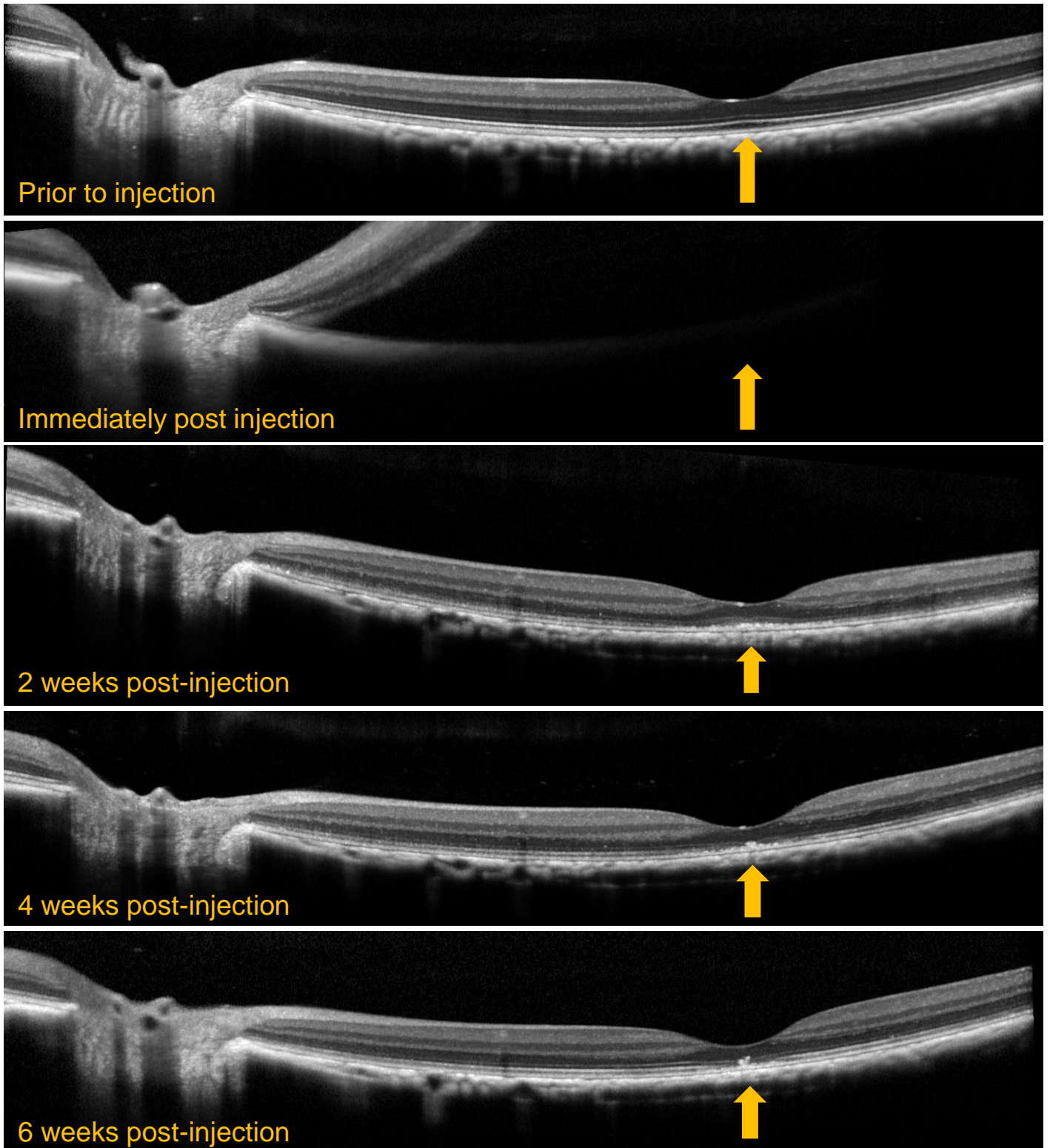


Figure S14. OCT scans from an eye that received a submacular SRI of AAV44.9-hGRK1-GFP. A loss of ellipsoid zone, and foveal bulge are present at 2 weeks post-injection. Structural abnormalities have not resolved by the study's end. Orange arrows demarcate location of foveal pit.

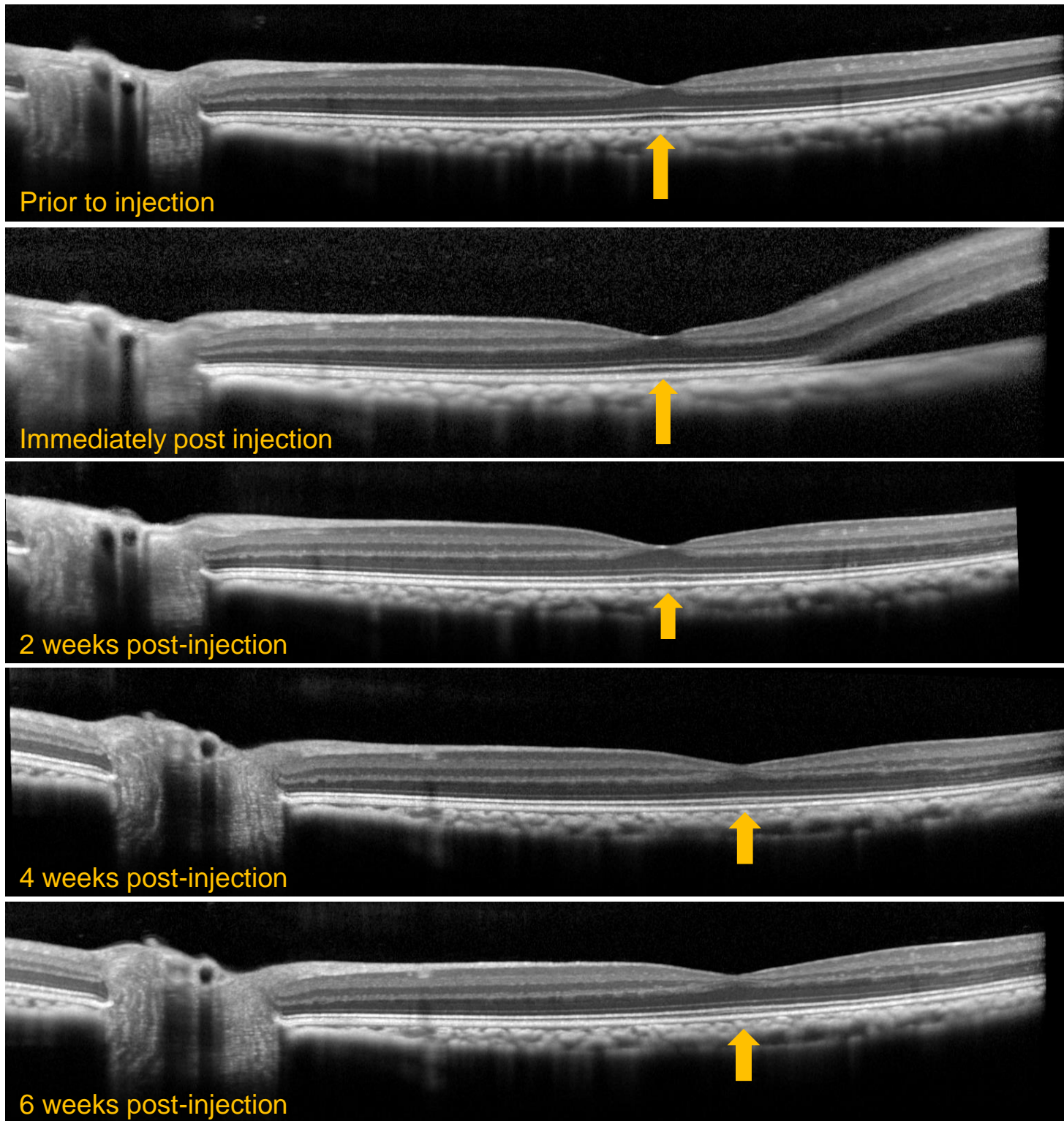


Figure S15. OCT scans from an eye that received a extrafoveal SRI of AAV44.9-hGRK1-GFP. No gross structural changes were observed in the fovea over the course of the study.

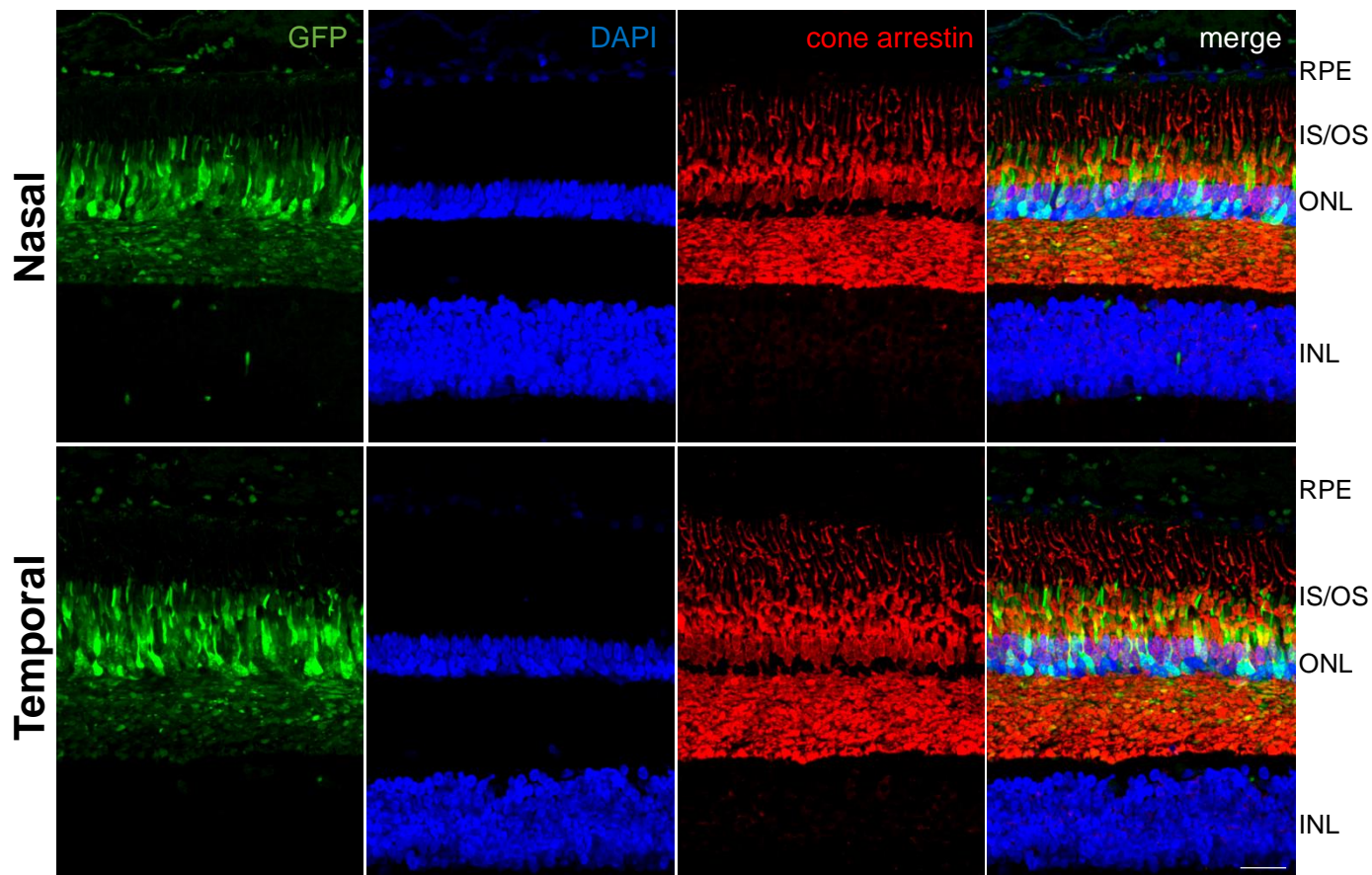


Figure S16. Retinal cross sections from macaque eyes that received extrafoveal subretinal injections (SRI) of AAV44.9(E531D)-hGRK1-GFP immunostained with an antibody raised against cone arrestin (red) and counter stained with DAPI (blue). Nasal and temporal parafoveal cones (~550 microns from foveal pit) express AAV44.9(E531D)- mediated GFP. 40X images are shown. Scale bar= 40 microns. RPE- retinal pigment epithelium, IS/OS- inner segments/outer segments, ONL- outer nuclear layer, INL- inner nuclear layer

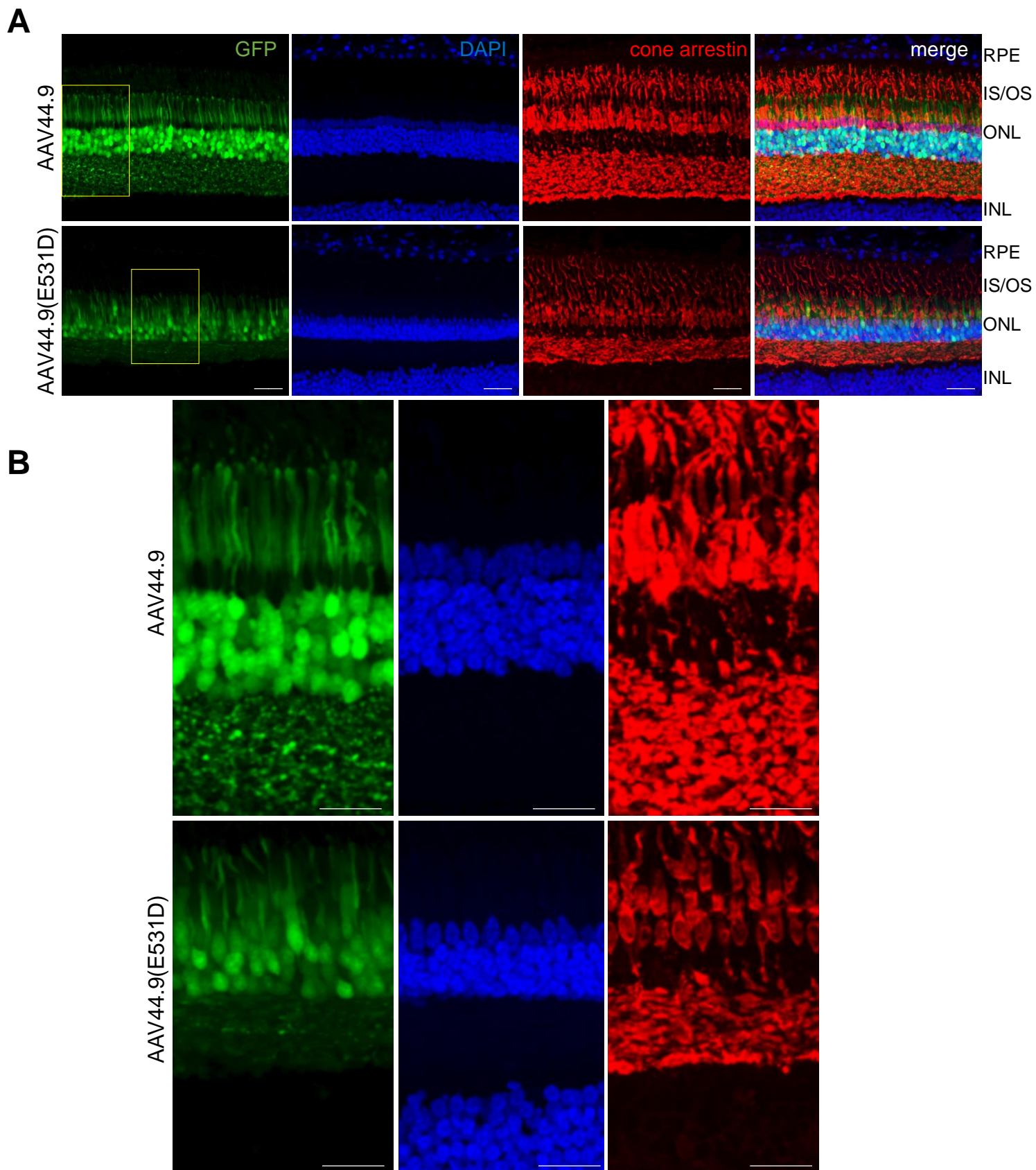


Figure S17. Retinal cross sections from macaque eyes that received extrafoveal subretinal injections (SRI) of AAV44.9-hGRK1-GFP (A,B- top row) or AAV44.9(E531D)-hGRK1-GFP (A,B- bottom row) were immunostained with an antibody raised against cone arrestin (red) and counter stained with DAPI (blue). GFP expression (green) was absent from perifoveal cones ($\sim 1100 \mu\text{M}$ nasal or temporal from the foveal pit) in eyes injected with AAV44.9. In contrast, perifoveal cones efficiently expressed AAV44.9(E531D)-mediated GFP. 20X (A, C) and 40X (C, D) images are shown. Scale bars in A= 40 microns, B= 20 microns. RPE- retinal pigment epithelium, IS/OS- inner segments/outer segments, ONL- outer nuclear layer, INL- inner nuclear layer.